

AFRL-SN-RS-TR-1999-268
Final Technical Report
January 2000



RADIO FREQUENCY PHOTONIC SYNTHESIZER

United Telecommunications Products, Inc.

Sponsored by
Defense Advanced Research Projects Agency
DARPA Order No. D965

APPROVED FOR PUBLIC RELEASE; DISTRIBUTION UNLIMITED.

The views and conclusions contained in this document are those of the authors and should not be interpreted as necessarily representing the official policies, either expressed or implied, of the Defense Advanced Research Projects Agency or the U.S. Government.

20000308 018

AIR FORCE RESEARCH LABORATORY
SENSORS DIRECTORATE
ROME RESEARCH SITE
ROME, NEW YORK

This report has been reviewed by the Air Force Research Laboratory, Information Directorate, Public Affairs Office (IFOIPA) and is releasable to the National Technical Information Service (NTIS). At NTIS it will be releasable to the general public, including foreign nations.

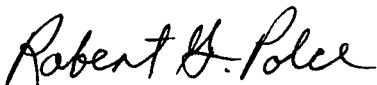
AFRL-SN-RS-TR-1999-268 has been reviewed and is approved for publication.

APPROVED:



JAMES E. NICHTER
Project Engineer

FOR THE DIRECTOR:



ROBERT G. POLCE, Chief
Rome Operations Office
Sensors Directorate

If your address has changed or if you wish to be removed from the Air Force Research Laboratory Rome Research Site mailing list, or if the addressee is no longer employed by your organization, please notify AFRL/SNDR, 25 Electronic Pky, Rome, NY 13441-4515. This will assist us in maintaining a current mailing list.

Do not return copies of this report unless contractual obligations or notices on a specific document require that it be returned.

RADIO FREQUENCY PHOTONIC SYNTHESIZER

Ronald T. Logan, Jr.
Ruo Ding Li

Contractor: United Telecommunications Products, Inc.
Contract Number: F30602-96-C-0272
Effective Date of Contract: 27 November 1996
Contract Expiration Date: 27 May 1998
Short Title of Work: Radio Frequency Photonic Synthesizer
Period of Work Covered: Nov 96 – May 98

Principal Investigator: Ronald T. Logan, Jr.
Phone: (215) 996-4761
AFRL Project Engineer: James E. Nichter
Phone: (315) 330-7423

Approved for public release; distribution unlimited.

This research was supported by the Defense Advanced Research Projects Agency of the Department of Defense and was monitored by James E. Nichter, AFRL/SNDR, 25 Electronic Pky, Rome, NY.

REPORT DOCUMENTATION PAGE			Form Approved OMB No. 0704-0188	
<small>Public reporting burden for this collection of information is estimated to average 1 hour per response, including the time for reviewing instructions, searching existing data sources, gathering and maintaining the data needed, and completing and reviewing the collection of information. Send comments regarding this burden estimate or any other aspect of this collection of information, including suggestions for reducing this burden, to Washington Headquarters Services, Directorate for Information Operations and Reports, 1215 Jefferson Davis Highway, Suite 1204, Arlington, VA 22202-4302, and to the Office of Management and Budget, Paperwork Reduction Project (0704-0188), Washington, DC 20503.</small>				
1. AGENCY USE ONLY (Leave blank)		2. REPORT DATE January 2000		3. REPORT TYPE AND DATES COVERED Final Nov 96 - May 98
4. TITLE AND SUBTITLE RADIO FREQUENCY PHOTONIC SYNTHESIZER			5. FUNDING NUMBERS C - F30602-96-C-0272 PE - 62712E PR - D965 TA - 00 WU - 02	
6. AUTHOR(S) Ronald t. Logan, Jr. and Ruo Ding Li				
7. PERFORMING ORGANIZATION NAME(S) AND ADDRESS(ES) United Telecommunications Products, Inc. Transmission System Division 500 Horizon Drive, Ste 502 Chalfont PA 18914			8. PERFORMING ORGANIZATION REPORT NUMBER N/A	
9. SPONSORING/MONITORING AGENCY NAME(S) AND ADDRESS(ES) Defense Advanced Research Projects Agency 3701 North Fairfax Drive Arlington VA 22203-1714			10. SPONSORING/MONITORING AGENCY REPORT NUMBER AFRL-SN-RS-TR-1999-268	
11. SUPPLEMENTARY NOTES AFRL Project Engineer: James E. Nichter/SNDR/(315) 330-7423				
12a. DISTRIBUTION AVAILABILITY STATEMENT Approved for public release; distribution unlimited.			12b. DISTRIBUTION CODE	
13. ABSTRACT (Maximum 200 words) An electro-optic device that synthesizes RF frequencies photonically by selection of two individual frequency pulses from a comb of frequencies generated by an actively mode-locked laser. The two frequencies are then combined (heterodyned) to produce the desired optical frequency source. The highly phase stable optical signal can be utilized in the photonic domain or detected for use as an electronic signal source. The prototype unit is rack mounted and computer controlled. The research conducted on this program verified the concept, produced a working prototype, and proposed the miniaturization of the photonic synthesizer.				
14. SUBJECT TERMS photonic, mode-locking, injection-locking, distributed-feedback (DFB) laser, synthesizer, phase noise, heterodyne			15. NUMBER OF PAGES 112	
17. SECURITY CLASSIFICATION OF REPORT UNCLASSIFIED			16. PRICE CODE	
18. SECURITY CLASSIFICATION OF THIS PAGE UNCLASSIFIED		19. SECURITY CLASSIFICATION OF ABSTRACT UNCLASSIFIED		20. LIMITATION OF ABSTRACT UL

Table of Contents

1. Executive Summary	1
2. Introduction	4
2.1 Background and Applications of the Photonic Synthesizer	4
2.2 Overview of Photonic Synthesizer Operation	6
2.3 Organization of the Report	8
3. Photonic Synthesizer Operation and Construction	10
3.1 Detailed Description of Operation	10
3.2 Prototype Design and Construction	12
3.3 Optical Spectrum Analyzer and RF Oscillator	19
3.4 Phase Noise Test Setup	24
3.5 Reference Oscillator Phase Noise	25
3.6 Photonic Synthesizer Measurement Technique	29
4. Theoretical Model	34
4.1 Introduction to injection-locking of semiconductor lasers	34
4.2 Analysis of DFB laser injection-locking	35
4.3 Stability analysis of injection-locking lasers	39
4.4 Experimental confirmation of injection-locking analysis	42
4.5 Phase noise analysis of injection-locking lasers	45
4.6 Residual phase noise of the Photonic Synthesizer	50
5. Experimental Results for Photonic Synthesizer Using Semiconductor Mode-Locked Laser	57
5.1 Construction of the semiconductor mode-locked laser	57
5.2 Performance of the semiconductor mode-locked laser	59
5.3 Phase Noise and timing jitter of actively mode-locked laser	62
5.4 Photonic Synthesizer proof-of-concept demonstration using semiconductor mode-locked laser	67
6. Photonic Synthesizer Experiments Using Fiber Mode-Locked Laser	73
6.1 Construction and performance of the fiber mode-locked laser	73
6.2 Performance of the Photonic Synthesizer using fiber mode-locked laser	77
7. Millimeter-wave Photonic Frequency Conversion Using Photonic Synthesizer	83
8. Summary and Conclusions	87
References	89
Acronyms	96

Table of Figures

Figure 1. Block diagram of the photonic synthesizer.	11
Figure 2. Optical spectrum of the mode-locked laser.	11
Figure 3. Frequency-domain picture of injection-locking of the DFBs to the mode-locked laser.	13
Figure 4. Photonic synthesizer optical configuration block diagram.	14
Figure 5. Absolute injection optical average power to the two DFB lasers as a function of Photonic Synthesizer chassis front monitor voltages.	15
Figure 6. Mechanical design illustration of Photonic Synthesizer.	16
Figure 7. Illustration of DFB laser packaging concept.	17
Figure 8. Laser optical power at the fiber output versus drive current.	18
Figure 9. Laser #2 frequency difference relative to laser #1.	20
Figure 10. Illustration of temperature tuning procedure for the DFB lasers to achieve a desired RF output frequency.	21
Figure 11. Optical spectrum analyzer based on Newport Supercavity TM high- finesse Fabry-Perot interferometer.	22
Figure 12. Block diagram of the Monitor Module internal configuration.	23
Figure 13. Configuration of the 1 GHz RF source used in the photonic synthesizer.	23
Figure 14. Conceptual block diagram of phase noise measurement system.	24
Figure 15. Typical HP 3048A phase noise measurement setup.	26
Figure 16. Phase Noise of our 100 MHz crystal oscillator using HP 3048A phase noise measurement system.	27
Figure 17. Phase noise of our 1GHz source constructed from Figure 13	28
Figure 18. Typical test setup for the photonic synthesizer, including the mode-locked laser, monitor module, and Photonic Synthesizer.	30
Figure 19. Single-sideband phase noise photonic synthesizer operated at 10 GHz.	31
Figure 20. Single-sideband phase noise of photonic synthesizer and HP83650L at frequency offset of 10kHz.	32
Figure 21. locking range as a function of the injection power to DFB slave laser output ratio, P_i/P (dB).	38
Figure 22. Stable and unstable injection-locking range as a function of injection power level.	42
Figure 23. Experimental setup used to measure the injection locking frequency range as a function of injection power level for two CW DFB lasers.	43
Figure 24. Experimental data and theoretical fit for the locking frequency range as a function of injection power level.	44
Figure 25. Illustration of optical spectrum analyzer display during the injection-locking experiments.	46
Figure 26. Measured oscillation frequency as a function of slave laser output power.	47
Figure 27. Photonic synthesizer residual phase noise $S_{res}(f)$ as a function of the locking range K .	53
Figure 28. Photonic synthesizer residual phase noise as a function of the detuning $\Delta\omega$ for locking range K of 500 MHz and 100 MHz.	54
Figure 29. Calculated SSB phase noise of the Photonic Synthesizer from Eq.(65)	56

Figure 30. Schematic diagram of actively mode-locked external cavity semiconductor laser.	57
Figure 31. Pulse profile of the external cavity semiconductor mode-locked laser, showing the minimum pulse width is about 15 ps at zero detuning.	59
Figure 32. RF spectrum of the semiconductor mode-locked laser.	60
Figure 33a. Mode structure of the semiconductor mode-locked laser.	61
Figure 33b. A zoom view in which individual modes are resolved.	61
Figure 34. Spectrum analyzer display of photodetected RF signal from mode-locked laser at 1 GHz.	64
Figure 35a. Phase noise of the 1GHz RF drive source used in the mode-locked laser.	66
Figure 35b. Phase noise of the mode-locked laser output at 1 GHz.	66
Figure 36. Residual phase noise of the semiconductor mode-locked laser at 1 GHz with RF driving source noise cancelled.	68
Figure 37. Block diagram of bench setup used for Photonic Synthesizer proof-of-concept demonstration using semiconductor external cavity mode-locked laser.	69
Figure 38. Signals generated from photonic synthesizer setup using the semiconductor mode-locked laser as master laser.	71
Figure 39. Zoom view of figure 38.	72
Figure 40. Schematic diagram of the fiber mode-locked laser used in the photonic synthesizer experiments.	74
Figure 41. RF spectrum of fiber mode-locked laser.	75
Figure 42a. Phase noise of the 1 GHz RF source.	76
Figure 42b. Phase noise of the fiber mode-locked laser at 1 GHz.	76
Figure 43. Residual phase noise of the fiber mode-locked laser at 1 GHz with RF driving source noise cancelled.	77
Figure 44. Experimental setup of the photonic synthesizer using the fiber mode-locked laser.	78
Figure 45. Phase noise of the photonic synthesizer at 18 GHz using the fiber mode-locked laser.	79
Figure 46. Millimeter wave signal at 50 GHz.	80
Figure 47. Comparison of RF phase noise at 10 kHz offset from carrier at different frequencies and sources.	81
Figure 48. Block diagram of photonic down-converter experiment using photonic synthesizer.	83
Figure 49. Block diagram of photonic down-converter experiment using photonic synthesizer as the optical local oscillator, and a wideband 50 GHz optical modulator as the photonic mixer.	84
Figure 50. Photonic synthesizer phase noise measurements at high frequencies of 60 GHz, and 94 GHz.	85

Table of Tables

Table 1. Reference Oscillator Phase Noise.	25
Table 2. Summary of Phase Noise Results.	33

1 Executive Summary

In this Final Technical Report, the first theoretical and experimental investigations are presented for a Photonic Synthesizer of radio frequency (RF) signals, previously proposed by the principal investigator of this study [1]. The Photonic Synthesizer utilizes a novel technique for RF optical heterodyne signal generation with high phase stability from near-DC through sub-millimeter-wave frequencies by the process of injection-locking two independently-tunable continuous-wave (CW) distributed-feedback (DFB) semiconductor laser diodes to the individual modes of the optical frequency comb generated by an actively mode-locked reference laser. The program goals to analyze and demonstrate the Photonic Synthesizer proof-of-concept were met, and performance goals for frequency range and phase noise were exceeded. In addition, a set of experiments was conducted that demonstrated an application of the Photonic Synthesizer as an optical local oscillator in a photonic RF frequency-converting fiber optic link at frequencies from 1 GHz to 94 GHz. This represents the widest frequency-range demonstration of RF photonic frequency conversion to date.

We first performed a systematic investigation to demonstrate the theoretical and experimental validity of the proposed photonic synthesis approach. First, we theoretically analyzed the optical injection-locking technique, establishing the locking conditions and stability for the DFB lasers in terms of parameters such as the ratio of injected optical power to DFB output power, injection-locking frequency range, and laser linewidth. We then performed experiments to validate our theoretical analysis. We worked closely with a subcontractor (Sarnoff) to design and fabricate novel high-power DFB laser diode chips with low noise and narrow linewidth, and to design and construct an actively mode-locked external cavity semiconductor laser. We characterized the lasers and then constructed a bench-top demonstration test bed of the Photonic Synthesizer and performed a successful concept demonstration that served to validate the theoretical predictions. We also demonstrated the Photonic Synthesizer using an actively mode-locked fiber ring laser (Pritel) based on Erbium/Ytterbium co-doped fiber.

After performing the theoretical analysis and bench demonstration, our activity focused on the design and construction of a deliverable packaged Photonic Synthesizer system in a series of standard 19" rack-mountable enclosures. The final hardware consisted of the Photonic Synthesizer, mode-locked fiber laser, a monitor module, laser diode controller, 1 GHz reference source, and a notebook computer and custom software to control the synthesizer.

Using the fiber ring mode-locked laser, high-quality microwave signals were generated from 1 GHz to 94 GHz, with phase noise less than -90 dBc at 10 kHz from a 50 GHz carrier. The phase noise from the Photonic Synthesizer was measured to be 15 to 20 dB lower than that of a commercially-available state-of-the-art 10 MHz to 50 GHz microwave synthesizer. The original goal of the program was to demonstrate phase noise performance comparable to a commercial wideband synthesizer at frequencies from 1 GHz to 50 GHz; this goal was exceeded by approximately 20 dB over the frequency range from 1 GHz to 94 GHz.

Finally, having achieved or exceeded the original program goals, we proceeded to demonstrate an RF photonic systems application of the Photonic Synthesizer in a millimeter-wave photonic frequency converting link. Signals from 60 GHz to 94 GHz were converted to frequencies less than 50 GHz in a single stage conversion using the Photonic Synthesizer as an optical local oscillator that fed a wideband optical modulator operated as a photonic mixer. We believe this to be the widest bandwidth demonstration to date of an RF frequency converting fiber optic link.

In summary, the Photonic Synthesizer concept was theoretically modeled and experimentally demonstrated. Measured performance was in good agreement with the theoretical expectations. While these results serve to validate the Photonic Synthesizer concept, further work remains to miniaturize the mode-locked laser and the core optical section of the Photonic Synthesizer as an optical integrated circuit in packaging suitable for military applications. This activity will require the development of novel approaches to optical integrated circuit (OIC) fabrication to combine multiple lasers, modulators, waveguides, optical gain elements, and a mode-locked laser onto a single OIC. The Photonic Synthesizer represents a truly novel low phase noise optical local oscillator over the frequency range from 1 GHz to 100 GHz that will enable the use of wideband photonic frequency converting links, which are expected to benefit many military and commercial applications at microwave and millimeter wave frequencies.

The authors wish to dedicate this work to the memory of the late Mr. Brian Hendrickson of DARPA, who initiated the funding for this research program at DARPA, but unfortunately passed away shortly after the program was started. His early and constant encouragement and generous support of this work are warmly appreciated. His friendship, technical insight, dedication, and leadership in developing RF photonic technology are deeply felt losses. We would like to believe he would have been pleased with the results reported here.

We also acknowledge the support and technical insight of James Nichter

of US Air Force Rome Laboratory (contract monitor), John Smith of DARPA, Edward Ackerman of MIT Lincoln Labs, Steve Pappert of US Navy SPAWAR, and Bill Burns of Naval Research Laboratory. We also acknowledge our close collaboration with and technical contributions of our subcontract partners at Sarnoff (Joseph Abeles and John Connolly) and Pritel (K.V. Reddy).

2 Introduction

2.1 Background and Applications of the Photonic Synthesizer

Optical techniques for microwave signal generation, distribution, and processing have attracted much interest in antenna-remoting, phased-array antenna beamforming, optical-microwave communication links, frequency converting fiber optic links, radio astronomy, and coherent communication systems. They also find applications in spectroscopy, atomic physics, metrology, and interferometry. A stable optical heterodyne signal generator would benefit many RF systems. Such a Photonic Synthesizer would be the optical equivalent of the traditional electronic frequency synthesizers employed in RF electronic systems, which would allow the use of optical heterodyne techniques in the processing of RF, microwave, and millimeter-wave signals using optical components instead of electronic components. This would allow fuller advantage to be taken of the inherently large RF bandwidth of optical fiber and optical components such as couplers, isolators, switches, attenuators, delay-lines, and optical amplifiers.

One obvious use of a heterodyne synthesizer is as a source of high-frequency local oscillator (LO) signals for distribution over an optical fiber network to multiple locations in a microwave or millimeter-wave system, such as a phased-array antenna. This would eliminate the need to generate high-frequency millimeter-wave LO signals from lower-frequency reference sources to drive down-convertors in the front-end areas of microwave and millimeter-wave antennas. The optical fiber medium has extremely low loss (<0.5 dB/km), so the signals could be distributed over tens of kilometers, and longer-distance distribution is possible using optical amplifiers. Also, a fiber-optic frequency distribution system offers extremely high electrical isolation between outputs, so that elements in the network can be added or subtracted without causing phase perturbations throughout the rest of the network.

Another promising application of the Photonic Synthesizer is as the optical LO source for a photonic RF frequency converting system [4, 5, 6, 8]. In one embodiment of a photonic frequency converting system, the heterodyne optical signal is used as the optical input to an intensity modulator that is driven by a microwave or millimeter-wave electrical input signal. The optical modulator multiplies the optical heterodyne signal with the electrical input signal, so that upon photodetection, the sum and difference frequencies between the electrical input and optical input signals are generated as

photocurrents. It has been shown theoretically and experimentally that the conversion loss of the heterodyne up-converted or down-converted signal is -6 dB compared to the unconverted RF signal [1, 4, 8]. The photonic frequency conversion system concept can potentially reduce the complexity of microwave and millimeter-wave systems, by eliminating much of the equipment required in the front-end area near the antenna aperture. A stable heterodyne optical source, such as the Photonic Synthesizer proposed here, is required to make the technique practical.

Optical heterodyne signals also find important applications in basic and applied research in many areas of spectroscopy and atomic physics [10]. Stimulated Raman transitions between two ground-states of atomic hyperfine levels have recently been used for atomic velocity selection and cooling at subrecoil temperatures [9], and have also been used for coherent wave-packet manipulation in an atom interferometer. Achieving these stimulated Raman transitions requires two counterpropagating frequency-stabilized laser beams detuned from an optical resonance by the RF hyperfine splitting frequency. The absolute linewidth of the laser is not important, but the relative linewidth of the two lasers must be small enough to drive coherent processes. For example, to use microwave signals to manipulate cesium atomic wave packets, an optical heterodyne system at a frequency offset of 9.2 GHz, the cesium clock frequency, is required.

Generation of RF optical heterodyne signals with low RF phase noise is non-trivial. Typically, an electronic phase-locked-loop (PLL) is required to keep the optical heterodyne beat locked to an external reference frequency. Without a feedback loop, the instantaneous linewidth of the millimeter-wave beat frequency generated by optical heterodyning is on the order of the individual laser linewidths, which are typically 5 - 10 kHz if Nd:YAG solid state lasers are used, and 1 - 10 MHz if DFB semiconductor lasers are used. This linewidth is three to six orders of magnitude larger than what is achievable by frequency multiplication of an electronic reference into the microwave frequency range. Also, slow frequency drifts of the absolute frequencies of the lasers ranging from several MHz to more than 1 GHz are superimposed on the instantaneous quantum-limited linewidth.

Previously, low-phase-noise heterodyne optical microwave and millimeter-wave signals have been generated by the process of heterodyne detection of the combined outputs of two single-frequency solid-state lasers with an optical frequency offset equal to the desired millimeter-wave signal. To obtain low phase noise at millimeter-wave frequencies, the feedback system requires a millimeter-wave electronic reference oscillator, millimeter-wave photodiode, amplifier, and phase detector. The frequency tuning range of

the lasers is typically much less than 100 GHz, and the actual heterodyne frequency locking range in which low-phase-noise operation may be obtained is typically limited to a much smaller range of frequencies by the electronic components in this control loop. Because of the difficulty of realizing a wideband PLL for microwave through millimeter-wave optical heterodyne generation, this technique has remained mostly a laboratory curiosity and is not widely employed in RF photonic systems applications.

Others have demonstrated injection-locking of independent laser diodes to a master laser diode that is injection-modulated to produce sidebands at harmonics of the modulation frequency. [2, 10, 15] Injection locking of a CW laser to an optical comb was previously investigated as a way to generate an extremely narrow channel spacing frequency-division-multiplexed (FDM) coherent optical communications system [14]. In these experiments, AM modulation was used to generate optical sidebands on a master laser, and optical injection locking was used to lock to these sidebands. However, the Photonic Synthesizer technique improves upon these earlier approaches, since the mode-locked laser provides an optical reference-frequency comb that spans a much wider range of frequencies with lower linewidth. This permits heterodyne signal generation over a wider frequency range with lower phase noise than previous techniques.

2.2 Overview of Photonic Synthesizer Operation

High phase stability is achieved in the Photonic Synthesizer by combining the outputs of two independently tunable "slave" lasers that are injection-locked to different optical modes of a "master" optical comb generated by an actively mode-locked laser. The slave lasers act as tunable narrow-band optical filters that pick out two modes of the reference frequency comb to produce a heterodyne output signal with very low phase noise. This technique transfers the frequency multiplication problem into the optical domain, so that heterodyne beat frequencies ranging from near-DC to greater than 100 GHz can be generated from a low-frequency electronic reference oscillator in a single compact system, approaching the theoretical minimum $20 \log(n)$ multiplication scaling law for phase noise. This eliminates the need for the complicated high-frequency electronic phase-locked-loops required by previous heterodyne signal generation techniques.

The mode-locked laser functions as an optical frequency reference that also performs the frequency-multiplication function in the optical domain. In the experimental system built and studied in this work, the mode-locked laser is driven by a low phase noise RF oscillator at 1 GHz. Therefore, the

optical mode spacing of the reference comb is 1 GHz.

The operation of the mode-locked laser can be understood as follows: In the absence of an electrical mode-locking input signal, the laser will operate in multiple longitudinal cavity modes with random phases between them. When a strong modulation of the gain from an external RF source is applied with frequency equal to the longitudinal cavity mode spacing, or a harmonic thereof, the previously randomly-fluctuating modes become phase-locked to each other. Each optical mode of the laser acquires sidebands due to the electrical modulation signal. When the frequency of the modulation signal equals the cavity mode spacing, the modulation sidebands mutually injection-lock the neighboring optical modes, causing all of the modes to establish a fixed phase relation between them. In this condition, the phase-locked modes cause the time-domain output to be a train of short pulses at a repetition rate equal to the mode-locking frequency. The width of the pulses is determined by the number of modes locked. Sub-picosecond pulses can be produced with mode-locked lasers, which requires that the locked optical modes span more than 1000 GHz of optical bandwidth.

For the Photonic Synthesizer, the phase of the detected RF heterodyne beat is determined only by the relative phases between the heterodyne frequencies. In the mode-locked laser, the relative phase between optical modes i and $i+m$ is equal to m -times the RF driving phase fluctuation [11, 12, 13]. There is also residual phase noise due to spontaneous emission, but our analysis indicates that it is generally very small compared with the phase noise of the RF drive signal, if the detuning between the RF frequency and mode-locked laser mode spacing is small. However, the residual phase noise could become significant and even larger than the RF source phase noise if the mode-locked laser is not properly locked. To obtain the lowest residual phase noise, in practice the mode locked laser cavity must be carefully stabilized to minimize any cavity fluctuation with respect to the RF drive frequency due to temperature fluctuations, mechanical vibrations, laser injection current variations, or other noise sources.

When optically-injection-locked, the phase fluctuations of the slave lasers follow the phase fluctuations of the master mode-locked laser [16, 20]. Due to the high correlation of the phase fluctuations of the individual modes of the mode-locked laser, a high-quality microwave to millimeter-wave signal is produced from the heterodyne beat of the two injection locked CW DFB lasers. Since the modes of the mode-locked laser can span over 1000 GHz of bandwidth, this technique can be employed to generate tunable microwave through sub-millimeter wave heterodyne optical signals with high phase stability.

To the best of our knowledge, the Photonic Synthesizer results reported here represent the first demonstration of optical injection locking of two CW DFB lasers to individual modes of a mode-locked laser to generate tunable microwave signals with low phase noise from 1 GHz to 94 GHz in a single apparatus.

2.3 Organization of the Report

The remainder of this report is organized as follows:

In Section 3, we describe in detail the principle of operation of the Photonic Synthesizer. The prototype design and construction is described, including the test setups used to characterize its performance. Also, the RF reference oscillator design, construction, and phase noise performance is detailed.

In Section 4, we present the results of theoretical calculations of expected phase noise for the system and its relation to important parameters in the design. The starting point is a detailed analysis of the optical injection locking technique using a theoretical model based on the laser rate equations.. From this analysis we then compute the expected phase noise of the Photonic Synthesizer, which rigorously establishes that the phase fluctuations of the DFB lasers follow the phase fluctuations of the mode locked laser. This result is important, since it establishes the theoretical model from which the detailed performance of the Photonic Synthesizer can be calculated and design trade-offs considered. We obtain the major design guidelines such as locking frequency range as a function of injection power, and also analyze the stability issues of injection locking.

In Sections 5 and 6, we present the main results of the Photonic Synthesizer experiments. Two types of mode-locked lasers were used in the experiments. The first is an external cavity actively mode-locked semiconductor laser. The other was an Erbium/Ytterbium co-doped optical fiber mode-locked laser.

In Section 5, we discuss the results of the initial proof-of-concept experiments for the Photonic Synthesizer using the external cavity semiconductor mode-locked laser. We first discuss the principle and construction of the mode-locked laser and the results of our characterizations, including pulse profile, RF spectrum, locking range, and tuning sensitivity. The phase noise of the resulting photodetected RF spectrum is presented and discussed.

Section 6 describes the main experimental results for the Photonic Synthesizer using the fiber mode-locked laser. Due to the superior stability of the fiber laser, these results represent the best performance achieved in this

research program. We first present details of the construction and results of our characterizations of the fiber mode-locked laser. Then, measurements of the Photonic Synthesizer are presented illustrating the generation of high quality microwave and millimeter-wave signals from 1 GHz to 94 GHz. The Photonic Synthesizer phase noise is compared with the phase noise of a state-of-the-art commercial signal generator (Hewlett-Packard HP83650L Synthesized Signal Generator) and we show that the Photonic Synthesizer has at least 15-20 dB lower phase noise over the 1 GHz to 50 GHz frequency range.. The results are found to be in good agreement with the theoretical predictions, thereby validating the theoretical model developed in this research program.

In Section 7, we present results of experiments conducted to demonstrate a wideband photonic frequency converting link using a 50 GHz optical intensity modulator. These results obtained were beyond the scope of the original program goals, and demonstrate the application of the Photonic Synthesizer as an optical LO source in a wideband photonic frequency converting system.

Finally, in Section 8, we discuss our conclusions and recommendations for further development. Possible improvements in the construction of the mode-locked laser, packaging of the Photonic Synthesizer, and control system issues are discussed.

3 Photonic Synthesizer Operation and Construction

3.1 Detailed Description of Operation

Fig.1 illustrates the principle of operation for the Photonic Synthesizer. The mode-locked laser is actively mode-locked by a high quality RF oscillator. The optical pulse train repetition rate is the same as the frequency of the RF oscillator. In the optical frequency domain, the frequency spacing between the modes equals the RF modulation frequency. The envelope of the modes has a Gaussian amplitude distribution in the frequency domain, and spans a region of optical frequency approximately equal to the inverse of the pulsewidth.

For optimum mode-locking, the cavity spacing of the mode-locked laser must be carefully adjusted such that it is the same as the RF oscillator frequency. In these experiments, a 1 GHz RF oscillator was used. Fig.2 shows the typical spectrum of the mode-locked laser output. For the external cavity semiconductor mode-locked laser, the minimum pulse width is achieved at zero detuning between the cavity mode frequency and the RF drive frequency, but this is accompanied by a relatively large amount of RF phase noise in the photodetected output. However, slight negative detuning between the cavity mode frequency and the RF drive frequency was found to minimize the phase noise. Previous work has shown that negative detuning suppresses cyclic instabilities in pulse-to-pulse amplitude [44]. We attribute the improved phase noise performance in the negative detuning condition to suppression of pulse-to-pulse jitter induced by the cyclic instabilities. Also, we found that the linewidth of the mode-locked laser in the minimum phase noise condition (negative detuning) was much reduced compared to the linewidth in the minimum pulse width condition (zero detuning). This result is also apparently related to the suppression of the cyclic instabilities.

For optimum performance, the RF reference oscillator used to drive the mode-locked laser must be a low phase noise oscillator, since any phase noise of the driving oscillator is translated to the mode-locked laser output [11, 12]. When properly mode-locked at the minimum phase noise condition, the phase noise of the photodetected output is typically limited by the RF source for frequencies within 10 kHz of the carrier.

When the optical pulse train from the mode-locked laser is injected into the CW DFB laser, the DFB laser can be phase-locked to that mode of the mode-locked laser, provided the injection-locking bandwidth of the DFB is smaller than the mode spacing of 1 GHz. Other modes outside the locking

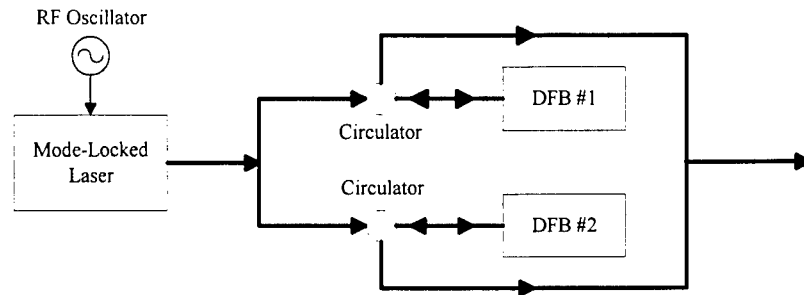


Figure 1: Block diagram of the photonic synthesizer. The mode-locked laser pulse train is split and injected into two DFB lasers. The DFB frequencies are tuned to be injection-locked to two modes of the mode-locked laser, thereby conferring a high degree of relative phase stability on the DFB outputs. Heterodyne photodetection of the combined DFB laser outputs generates microwave signals with low phase noise.

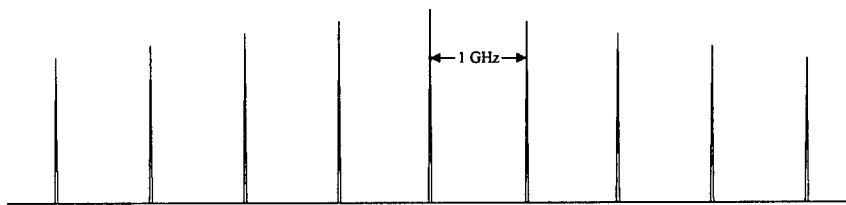


Figure 2: Optical spectrum of the mode-locked laser, showing the 1 GHz mode spacing, which is equal to the RF oscillator frequency used to mode-lock the laser.

range will introduce phase modulation on the DFB laser. As the locking bandwidth of the DFB laser is decreased, these phase modulations become smaller. However, if the DFB laser locking bandwidth is too small, locking the slave laser to the desired mode becomes more difficult, particularly if either the mode-locked laser comb fluctuates in the frequency domain, or if the DFB laser frequency fluctuates. The optimum locking bandwidth is determined from the experiments as a compromise between the stability of injection locking and the sideband suppression.

In the Photonic Synthesizer setup, the mode-locked laser is split and simultaneously injected into two DFB lasers as shown in Fig.1. When the free-running frequency of DFB laser #1 is adjusted within the locking range of the i th mode of the mode-locked laser, and laser #2 is adjusted within the locking range of the j th mode of the mode-locked laser, the DFB lasers will be injection-locked to i th and j th modes of mode-locked laser, respectively. Thus the frequency difference between laser #1 and laser #2 is precisely set to the frequency difference of i th and j th modes of the mode-locked laser, which is an integral multiple of the modulation frequency of the RF oscillator. The phases of the slave lasers also assume the same phases as the i th and j th modes of mode-locked laser. The photodetected heterodyne combination of the two DFB lasers is a low phase noise RF signal. This is illustrated in Fig.3 where a 4 GHz signal is generated as an example.

In this way, coarse tuning in 1 GHz steps is used to generate low phase noise heterodyne signals from 1 GHz to over 100 GHz. To interpolate between the 1 GHz modes to achieve finer frequency resolution, one of the DFB modes may be frequency shifted prior to heterodyne combination. The frequency shifting can be achieved using standard acousto-optic modulation or electro-optic modulation techniques. Then the phase noise of the resulting heterodyne signal is determined fundamentally by the multiplied phase noise of the 1 GHz reference oscillator, plus any phase noise due to the interpolating signal. At high frequencies, the multiplied 1 GHz phase noise will typically limit the performance.

3.2 Prototype Design and Construction

In this section, we focus on design and construction issues related to the Photonic Synthesizer prototype. We will discuss the theoretical and experimental results for the mode-locked laser, injection locked DFB lasers, and the phase noise of the Photonic Synthesizer in following sections.

The core of the Photonic Synthesizer prototype is constructed using polarization-maintaining (PM) single-mode optical fiber components. PM

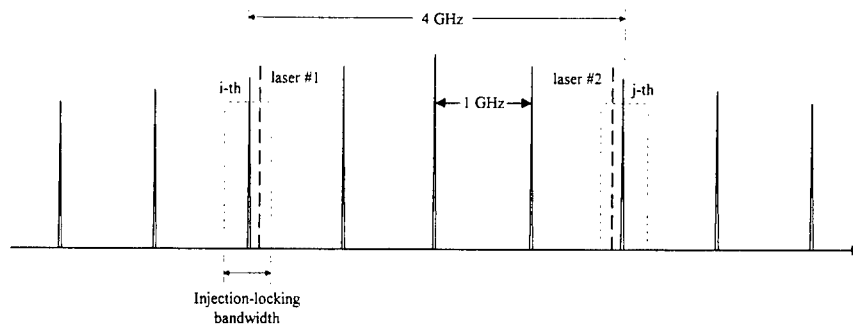


Figure 3: Frequency-domain picture of injection-locking of the DFBs to the mode-locked laser. The mode-locked laser output is injected into DFB laser #1 and DFB laser #2. Laser #1 is tuned to within the locking range of the i -th mode of the mode-locked laser, and laser #2 is tuned to the j -th mode locking range, as indicated in the long dashed line when they are in free-running situation. When injected by the mode-locked laser, lasers #1 and #2 become phase locked to the i -th and j -th modes respectively. Therefore, their beat generates an RF signal upon photodetection (in this case, at 4 GHz.)

components are required because both injection-locking and optical heterodyne signal generation require that the optical signal polarization be preserved. The detailed implementation of the Photonic Synthesizer is illustrated in the block diagram of Fig.4. It is noted that the goal of the research program was to build a proof-of-concept prototype using available components. Ideally, many of the components of the synthesizer would be contained in a single integrated optical circuit, which would reduce or eliminate the need for PM optical fibers, couplers, isolators, modulators, etc, since polarization can be more easily managed in integrated optical waveguides.

Referring to Fig. 4, we now describe the signal flow through the system. The mode-locked laser output is split by a 50/50 PM splitter, which provides the input signals to injection lock the DFB lasers. These signals pass through optical isolators to reduce reflection back into the mode-locked laser cavity to minimize instabilities. Each signal then passes through a lithium-niobate integrated Mach-Zehnder optical modulator which is part of an automatic level control (ALC) circuit that keeps the optical injection power constant. The ALC circuit is comprised of a 10% optical coupler, DC photodetector,

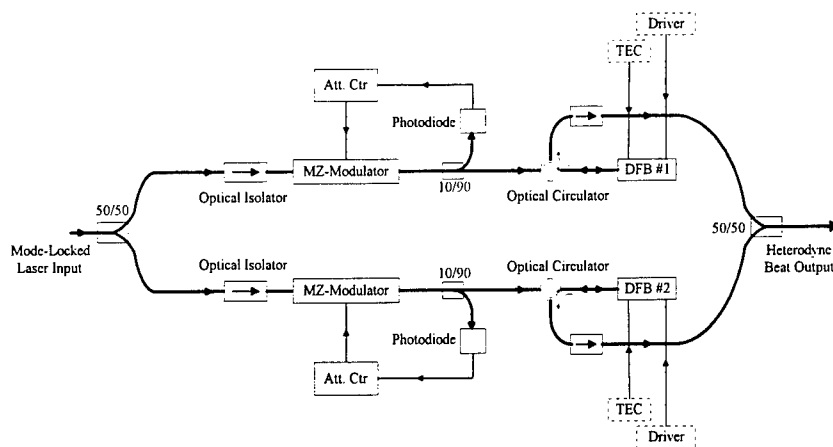


Figure 4: Photonic synthesizer optical configuration block digram.

transimpedance amplifier, and negative feedback circuit that controls the DC bias of the modulator to maintain a constant optical power. In the final deliverable unit, the DC levels of the two ALC photodetectors can be monitored on the front panel of the Photonic Synthesizer. This permits adjustment of the injection level of the mode-locked laser to the two DFB lasers. Fig.5 shows the corresponding injection optical average powers to the DFB lasers versus the DC monitor voltages on the front panel.

In all of the experiments, the DFB lasers are coupled via one facet using an optical circulator to simplify the optical alignment and packaging. Following the optical circulators, two more optical isolators are used to minimize possible backreflections into the DFB lasers or mode-locked laser which may introduce further instabilities. Finally, the two optical outputs from the DFB lasers are combined in a second 50/50 PM optical coupler to produce the desired optical heterodyne beat signal. The coupling ratio could be varied with a micrometer which permitted fine adjustment to equalize the output powers of the two lasers in the final heterodyne output to achieve maximum photodetected RF signal amplitude.

The output phase of the RF heterodyne signal is degraded by fluctuations caused by changes in relative optical length between the two optical paths through the DFB laser. To minimize these drifts, the prototype is constructed on a thermally-controlled aluminium plate. The plate is mounted on an array of thermoelectric cooler (TEC) modules which are controlled to maintain the plate at constant temperature of 30° C. The optical fibers

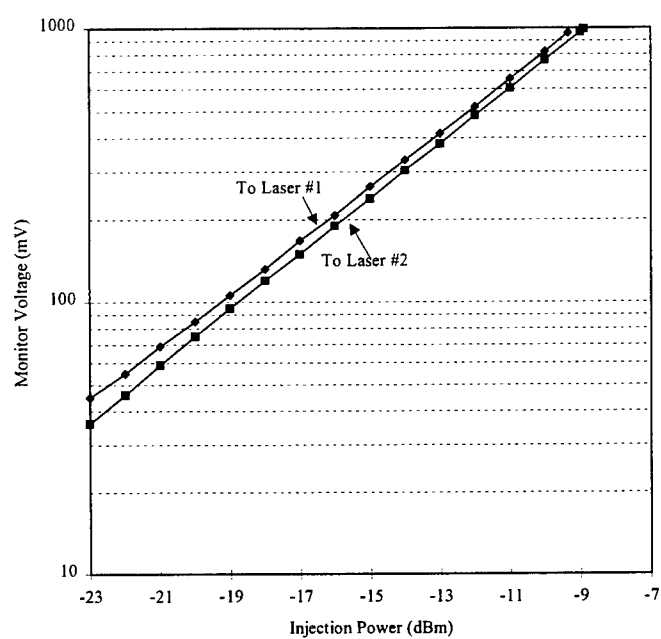


Figure 5: Absolute injection optical average power to the two DFB lasers as a function of Photonic Synthesizer chassis front panel monitor voltages.

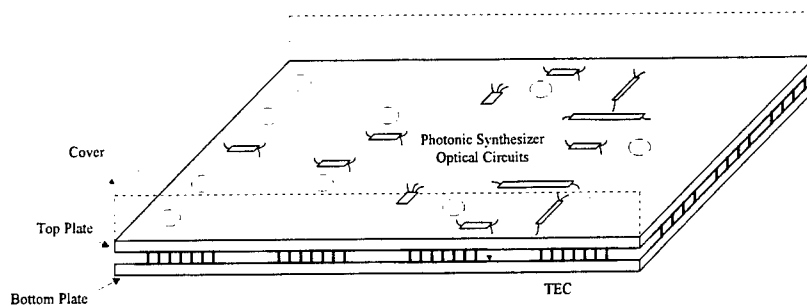


Figure 6: Mechanical design illustration of Photonic Synthesizer. The top aluminium plate hosts all optical components and fiber management. The plate rests on a grid of TEC modules which keep the plate at constant temperature using a feedback circuit. The thermal sensors for the feedback circuit are embedded in the plate. The bottom plate of the chassis provides the thermal sink for the TECs. The top plate is covered by a rigid nylon enclosure to reduce airflow over the components.

connecting the components are kept in close contact with the plate as well. Finally, the plate is covered by a nylon enclosure to minimize air flow over the components. The optical fibers connecting the components are carefully spliced such that the length difference between the upper path and lower path in Fig.4 is within 0.25 inches. This is important to minimize any noise added due to phase discrimination from path differences in the coherent heterodyne system. The Photonic Synthesizer also includes all the electric circuitry to automatically maintain the temperature for the plate. Fig.6 displays the illustration of the mechanical design of Photonic Synthesizer. It is noted that such drastic precautions to control the temperature of the optical paths would probably not be necessary for a monolithically-integrated Photonic Synthesizer optical circuit.

The DFB lasers used in the Photonic Synthesizer have output power of approximately 80 mW ex-facet, linewidth of less than 1 MHz, and low relative intensity noise (RIN) less than -165 dBc/Hz at frequencies below 1 GHz. The DFB chips were designed and fabricated by Sarnoff Research Center. The lasers were packaged in standard 14-pin butterfly packages on thermo-electric coolers, with special care taken to minimize reflections into the laser cavity. Fig.7 illustrates the laser packaging concept used. Instead of a conventional DFB package where an optical lens and isolator are used prior to fiber launch, the fiber tip was polished to produce a lensed fiber

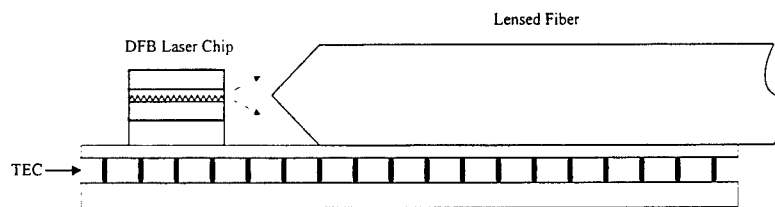


Figure 7: Illustration of DFB laser packaging concept. The fiber tip was polished to create a lens to couple the laser chip output to the fiber with minimum back-reflection. The fiber is metallized and soldered directly to the same ceramic substrate as the DFB laser chip. No optical isolator is used, since the input and output are taken from the same facet of the chip.

which directly collects the light from DFB laser chip output. The fiber is metallized and soldered to the same ceramic alumina substrate as the laser chip, which is then attached to the thermo-electric cooler. The lensed fiber tip minimizes the back reflection to the laser chip to prevent laser instability. The soldered construction minimizes movement of the chip relative to the fiber tip as the chip temperature is varied to tune the wavelength. A thermistor and back-facet monitor photodiode are also mounted to the alumina substrate. The coupling efficiency to the fiber was estimated to be on the order of 20% to 30%. Although this is lower coupling efficiency than can be achieved using a lens, the benefit of minimum back reflection was determined to be more important for the purposes of demonstrating the Photonic Synthesizer concept. Maximizing the coupling efficiency of the DFBs and determining permissible levels of back-reflection without degrading the performance of the Photonic Synthesizer remain as topics for future study. Fig.8 shows the laser power at the fiber output vs. driving current for the butterfly package. The power levels obtained with this package were adequate for the Photonic Synthesizer experiments.

The two DFB lasers were controlled by an ILX Lightwave LDX-3100 laser diode controller which provided laser current and temperature control. Coarse tuning of the DFB frequencies was accomplished by varying the chip temperature with the thermo-electric cooler, while fine adjustments could be made by varying the laser current. The lasers were first selected to have wavelengths as close as possible when operated at the same temperature. Then careful measurements were made of optical frequency versus chip temperature at constant current. The temperature and current of DFB laser #1 was fixed at 22.9 °C and 260 mA respectively, and its absolute frequency

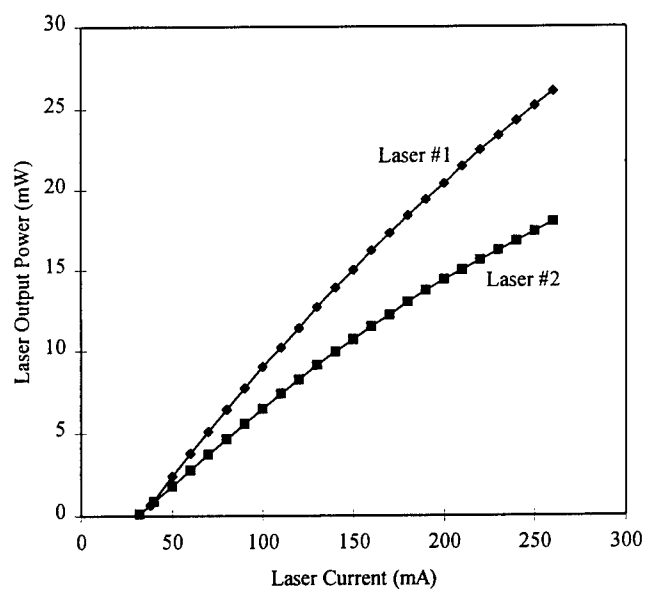


Figure 8: Laser optical power at the fiber output versus drive current.

was measured. Absolute optical frequency measurements were taken using a Burleigh WavemeterTM with 30 MHz accuracy. Then we measured the frequency of DFB laser #2 at constant value of 249 mA relative to laser #1 while varying the temperature of laser #2. Fig.9 shows the results of these measurements, which show that the laser frequency changed linearly versus temperature, with a slope of approximately 14 GHz / °C. This measurement was repeated 11 times for each DFB laser to determine the repeatability of the laser frequency versus operating temperature. It was found that the standard deviation of the optical frequency at a given temperature is within 200 MHz. The high repeatability of the laser frequency versus temperature was exploited to simplify the control software for tuning the Photonic Synthesizer. The laser chip temperature could be reliably controlled with 0.1 °C resolution, which yielded tuning resolution of approximately 1.4 GHz.

Adjustment of the laser temperature alone did not yield enough resolution to tune the laser frequency within the injection-locking range of a desired mode, which is less than 1 GHz. So, after the temperature was tuned so that the DFB frequency was close to the desired mode of the mode locked laser, the laser current was adjusted slightly to precisely align the laser frequency with the mode as illustrated in Fig.3. For the DFB lasers used, the tuning coefficient of laser frequency versus current was approximately 200 MHz / mA. The DFB current could be controlled to increments of 0.1 mA, yielding 20 MHz of tuning resolution. In our experimental setup, the absolute frequency of the mode-locked laser modes drifted with time, due to thermal drift of the cavity. This drift of the mode-locked laser frequency, combined with the 200 MHz standard deviation of the DFB laser frequency versus temperature, necessitated manual tuning of the DFB laser current to precisely align the DFB lasers to the mode-locked laser modes to achieve proper injection-locking. Fig.10 illustrates an example of tuning DFB laser #2 away from DFB #1 by approximately 20 GHz, and then 50 GHz, when the temperature is changed from 23.6 °C to 25.8 °C. It is noted that elimination of the manual tuning requirement must be addressed in future research and development. However, an integrated optical approach for both the Photonic Synthesizer is expected to result in less relative drift between the optical paths, since the entire assembly can then be temperature-stabilized.

3.3 Optical Spectrum Analyzer and RF Oscillator

A Newport SupercavityTM Fabry-Perot interferometer was used to analyze the optical spectrum of the Photonic Synthesizer and to assist in the tuning

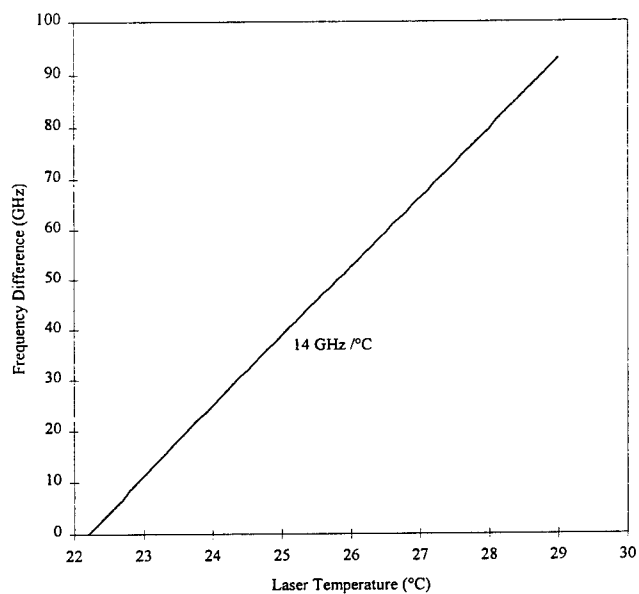


Figure 9: Laser #2 frequency difference relative to laser #1. Laser #1 operates at 260 mA and 22.9 °C. Laser #2 current is fixed at 249 mA. This shows that the laser frequency changes linearly with temperature with tuning coefficient of approximately 14 GHz / °C.

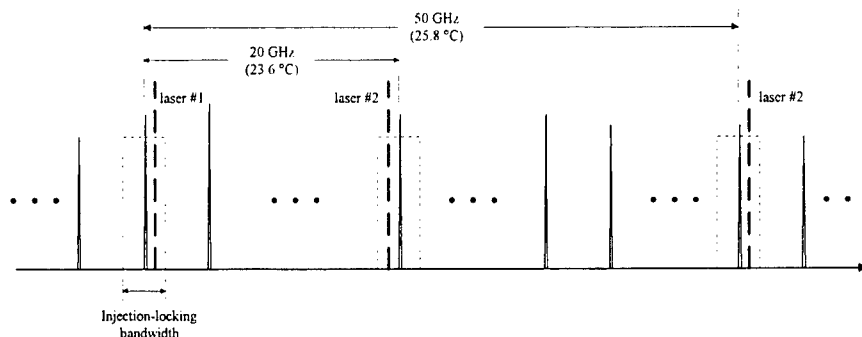


Figure 10: Illustration of temperature tuning procedure for the DFB lasers to achieve a desired RF output frequency. Laser #1 operates at constant current of 260 mA and constant temperature of 22.9 °C. Laser #2 is tuned by changing its temperature. In the figure, laser #2 frequency difference relative to laser #1 is tuned close to 20 GHz when temperature is at 23.6 °C, and close to 50 GHz when temperature is tuned to 25.8 °C.

of the DFB slave lasers to achieve injection locking as illustrated in Fig.10. The interferometer was custom-specified and fabricated to have a high finesse $F > 10,000$, a free spectral range of 500 GHz, and resolution of approximately 50 MHz, thus permitting resolution of the mode structure of the mode-locked laser with mode spacing of 1 GHz over the 100 GHz operating range. As the cavity was not fiber-coupled, a free-space optical train was constructed to match the optical mode of a collimated single-mode fiber output to the mode of the SupercavityTM, as illustrated in Fig.11.

A separate 19-inch rack-mountable chassis, called the Monitor Module, was constructed to contain the SupercavityTM spectrum analyzer and optics as shown in Fig.11, and also some optical couplers and an optical isolator. The configuration of the Monitor Module is displayed in Fig. 12. Two optical splitters with 1% and 10% coupling ratios tap the output from the Photonic Synthesizer and mode-locked laser. The tapped outputs can be sent to the SupercavityTM optical spectrum analyzer through a 4×1 coupler. An optical isolator is used to prevent reflections from the Supercavity back into the lasers. Fig.12 shows the internal configuration corresponding to the labels used on the front panel of the Monitor Module.

The 1 GHz RF source required to mode-lock the laser is also contained inside the Monitor Module. One critical parameter for this RF source is low phase noise. Any phase noise from this RF source will directly translate to

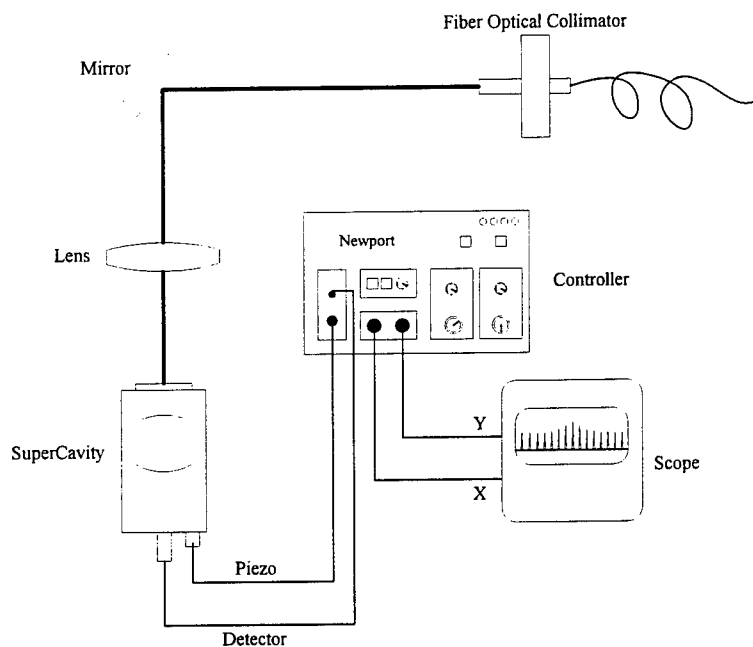


Figure 11: Optical spectrum analyzer based on the Newport SupercavityTM high-finesse Fabry-Perot interferometer. The single-mode fiber optic input is transformed to a collimated free-space beam by a GRIN lens. A second condensing lens focuses the beam into the Supercavity. The distances from the fiber optical collimator to the lens, and from the lens to the Supercavity input, as well as the focus length of the lens were selected carefully to achieve proper mode-matching to the SupercavityTM.

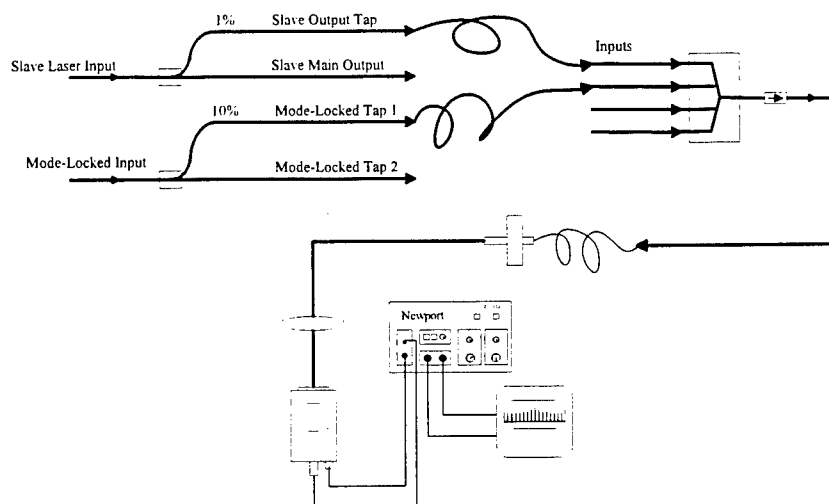


Figure 12: Block diagram of the Monitor Module internal configuration, showing labels as they appear on the front panel of the 19-inch rack mountable chassis.

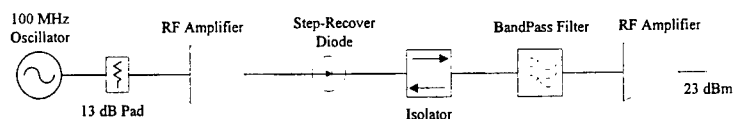


Figure 13: Configuration of the 1 GHz RF source used in the photonic synthesizer.

phase noise in the mode-locked laser, which will ultimately limit the phase noise performance of the Photonic Synthesizer.

A 1 GHz RF source was constructed starting from a very low phase noise, oven-controlled 100 MHz quartz crystal oscillator. The output of the oscillator was amplified, then used to drive a step-recovery-diode to generate a frequency comb to about 2 GHz with spacing of 100 MHz. The desired 1 GHz tone was passed by a narrow bandpass filter, which suppressed the other harmonics. Finally, this 1 GHz signal was amplified to approximately +23 dBm and used to drive the mode-locked laser. Fig. 13 illustrates the configuration of the 1 GHz RF source.

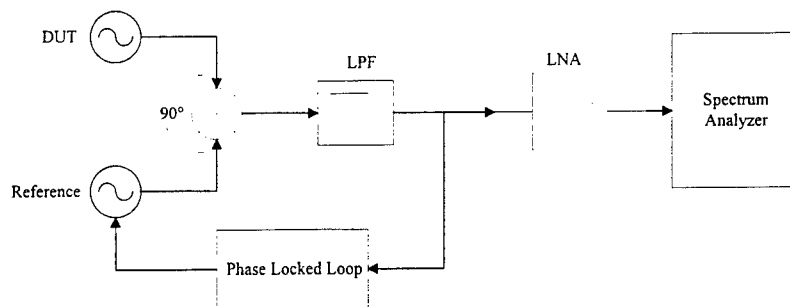


Figure 14: Conceptual block diagram of phase noise measurement system.

3.4 Phase Noise Test Setup

Before discussing the phase noise measurement results of this RF source, a brief introduction of the phase noise test setup used in most of the measurements is presented. A Hewlett-Packard HP 3048A phase noise measurement system was employed for measurements at 1 GHz and below, while the internal phase noise measurement capability of an HP8565E 50 GHz RF spectrum analyzer was used for most of the microwave frequency measurements. The basic principle of operation of the HP 3048A system is illustrated in Fig.14. The signals from the device under test (DUT) and reference source enter the double-balanced mixer. The two signals are kept at quadrature phase (90° out-of-phase) by a PLL feedback loop that tunes the reference oscillator. In this configuration, the mixer IF output is a voltage that is linearly proportional to the phase difference between the inputs, provided the difference is less than about 10 degrees. The power spectrum of the IF output is equivalent to the phase noise of the DUT, provided that the reference oscillator phase noise is much lower. The low pass filter (LPF) prevents LO feedthrough and mixer sum products from overloading the low noise amplifier. The low noise amplifier (LNA) improves the sensitivity and noise figure of the spectrum analyzer.

Fig.15 shows the instruments and configuration used in the HP 3048A system. The HP 11848A phase noise interface contains a double-balanced mixer used as a phase detector operating from 5 MHz to 1.6 GHz frequency range, a low pass band filter, a low noise amplifier, and a phase-locked-loop. The mixer L port is the input of the reference source, while the R port is the input of the DUT. The phase detector output is sent to an HP 3561A dynamic signal analyzer. We choose a low phase noise HP 8662A synthesizer

as our reference source. The system also includes a HP 70427A microwave downconverter to extend the frequency to 26 GHz. A typical configuration to measure absolute phase noise of DUT is shown in Fig.15.

3.5 Reference Oscillator Phase Noise

Fig. 16 displays the phase noise measurement of the 100 MHz oscillator used in our 1 GHz source as outlined in Fig.13. In this case, due to the very low phase noise of our 100 MHz oscillator, which was significantly lower than the HP 8662A synthesizer reference, we instead used an identical 100 MHz oscillator as the reference, so that we measured the two oscillators against each other. So in the setup outlined in Fig.15, instead of using the HP 8662A synthesizer in port L, we used two independent 100 MHz oscillators at both port L and port R. Since our oscillators could be tuned by varying a DC control voltage we connected the voltage tuning port to the phase noise interface to tune the oscillator during the phase noise measurement, thus compensating for frequency drift. In this type of measurement, it is assumed that the two oscillators have identical phase noise, so that the displayed phase noise level is the sum of two independent random processes. Therefore, it assumed that the individual oscillator phase noise is a factor of two lower, or -3 dB.

Similar phase noise measurements were performed for the two identical 1 GHz multiplied sources of the configuration in Fig.13. Fig. 17 displays these results. The phase noise of our 1 GHz source is among the lowest available from commercial vendors. Table 1 summarizes the phase noise for the 100 MHz and 1 GHz RF sources used in the Photonic Synthesizer project. The harmonics visible in the phase noise plots are assumed to be due to spurious 60 Hz noise and harmonics thereof. No excessive measures were taken to reduce this noise source in these measurements.

Table-1: Reference Oscillator Phase Noise		
SSB Phase Noise PSD [dBc/Hz]		
Offset	100 MHz Oscillator	1 GHz Source
100 Hz	-123	-100
1 kHz	-150	-125
10 kHz	-170	-135
100 kHz	-175	-140

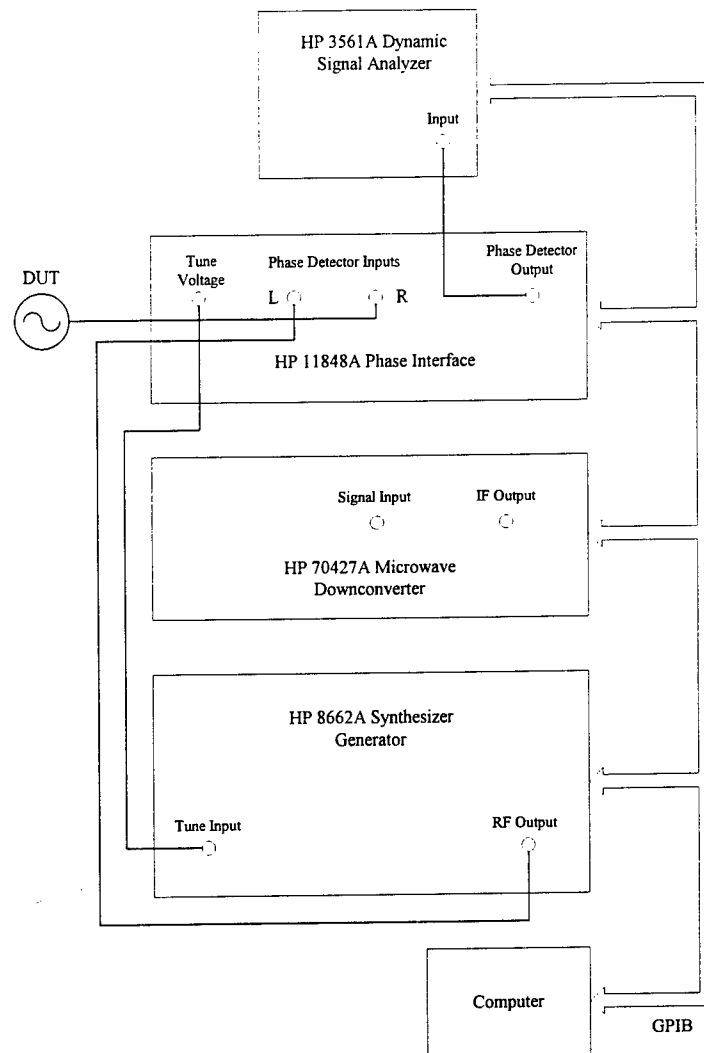


Figure 15: Typical HP 3048A phase noise measurement setup.

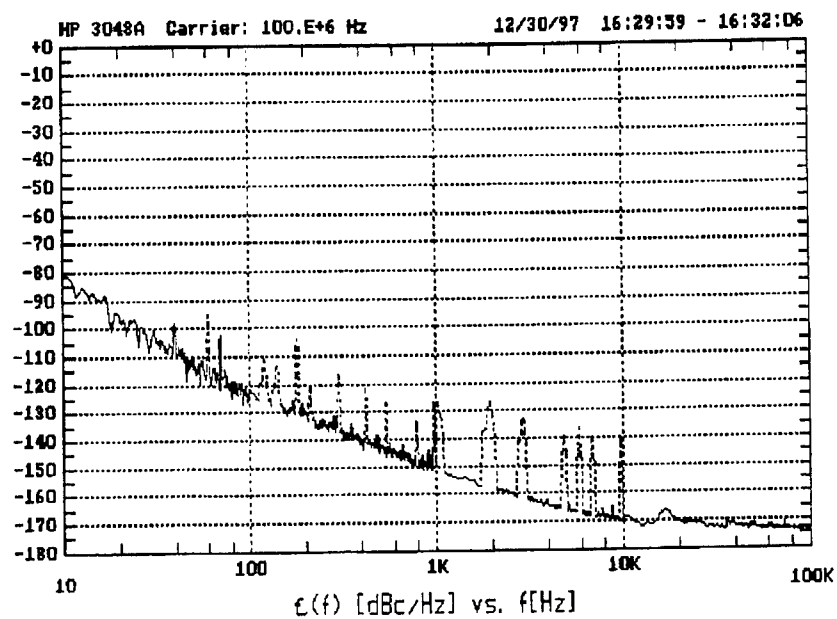


Figure 16: Phase noise of our 100 MHz crystal oscillator measured using HP 3048A phase noise measurement system. In this measurement, a pair of 100 MHz oscillators are used.

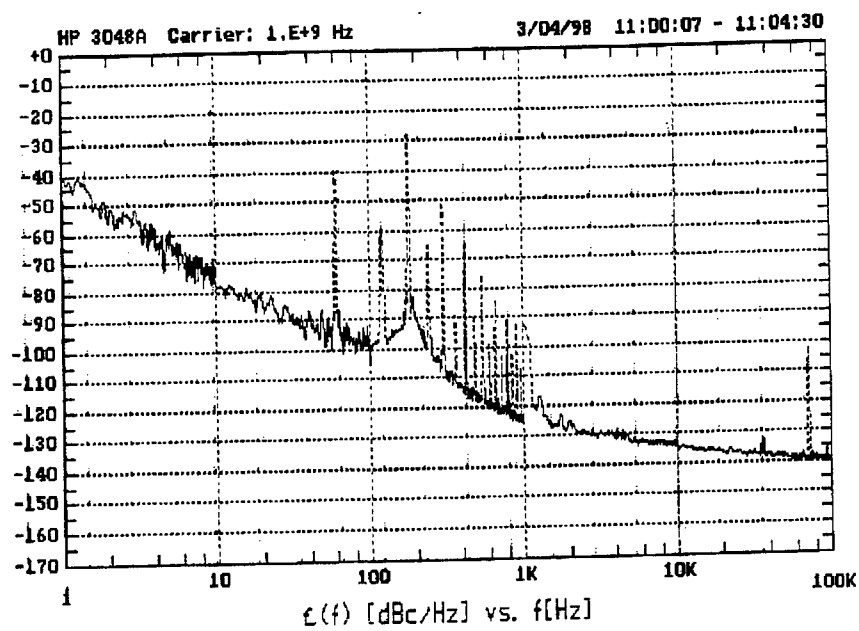


Figure 17: Phase noise of our 1 GHz source constructed from Fig.13. A pair of such sources are used to measure their phase noise.

3.6 Photonic Synthesizer Measurement Technique

To aid the reader in understanding the upcoming detailed discussion of the mode-locked laser, injection-locking technique, and Photonic Synthesizer performance in the following sections, we will first give a brief introduction to the measurement setup and techniques we used to operate and characterize the Photonic Synthesizer prototype. Fig.18 displays the typical setup we used for testing the Photonic Synthesizer, which we will now describe. Starting from mode-locked laser, the RF source at 1 GHz which resides in the Monitor Module (bottom left) provides the reference input to the mode-locked laser. The mode-locked laser has two main outputs: output #1 (the primary output) has output power of approximately +13 dBm via a polarization-maintaining (PM) fiber-optic connector. This output is directed to the input of the Photonic Synthesizer through a PM fiber cable. Another output of the mode-locked laser (auxiliary output) has output power of +17 dBm and is sent to the Monitor Module mode-locked laser input port. The output from the Photonic Synthesizer is directed to the slave laser input port of the Monitor Module. In the Monitor Module, a portion of the mode-locked laser output is combined with a portion of the Photonic Synthesizer output, which is then input to the SupercavityTM optical spectrum analyzer. This permits display of the mode-locked laser and Photonic Synthesizer optical modes simultaneously on an oscilloscope to assist the laser tuning for optimum injection locking. The remaining large part of the mode-locked laser output is detected by a high-speed photodetector and monitored using a 50 GHz RF spectrum analyzer. The RF comb produced by the photodetected mode-locked-laser pulse train is observed to insure that the mode-locked laser is properly mode-locked with minimum RF noise. From time to time, the mode-locked laser cavity length must typically be adjusted to ensure its optimum operation. About +9 dBm from the remaining part of the Photonic Synthesizer output is detected by another high-speed photodetector. This output is amplified and used to perform phase noise measurements using a Hewlett-Packard HP3048A phase noise measurement system as outlined in the Fig.15. This output is also viewed on an RF spectrum analyzer to observe the generated RF, microwave and millimeter-wave signals, and to measure the high-frequency phase noise.

Although a more detailed discussion and presentation of the phase noise results of the Photonic Synthesizer will be presented in following Sections, here we present an example of such measurements and a condensed summary of the phase noise at different frequencies. Fig.19 shows the phase noise test result of the Photonic Synthesizer at 10 GHz vs. offset frequency from the

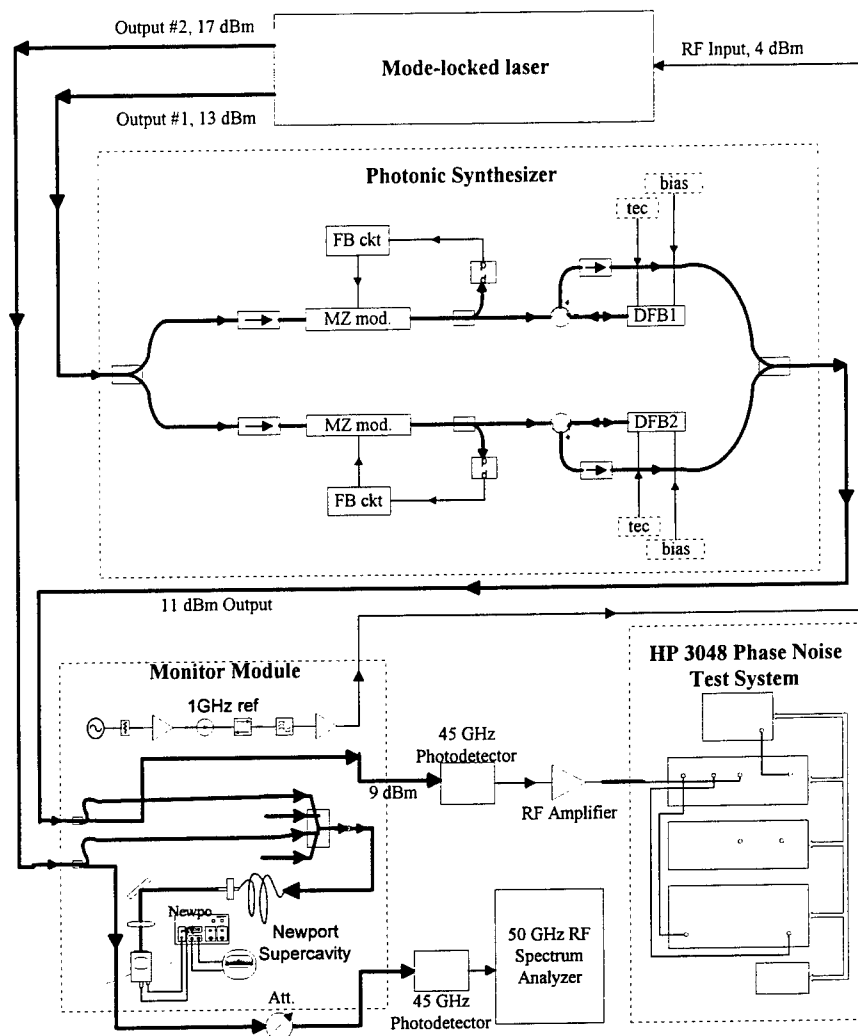


Figure 18: Typical test setup for the photonic synthesizer, including the mode-locked laser, monitor module, and Photonic Synthesizer. The HP3048A phase noise measurement system and a 50 GHz HP8565E RF spectrum analyzer are used to examine the detected optical heterodyne output.

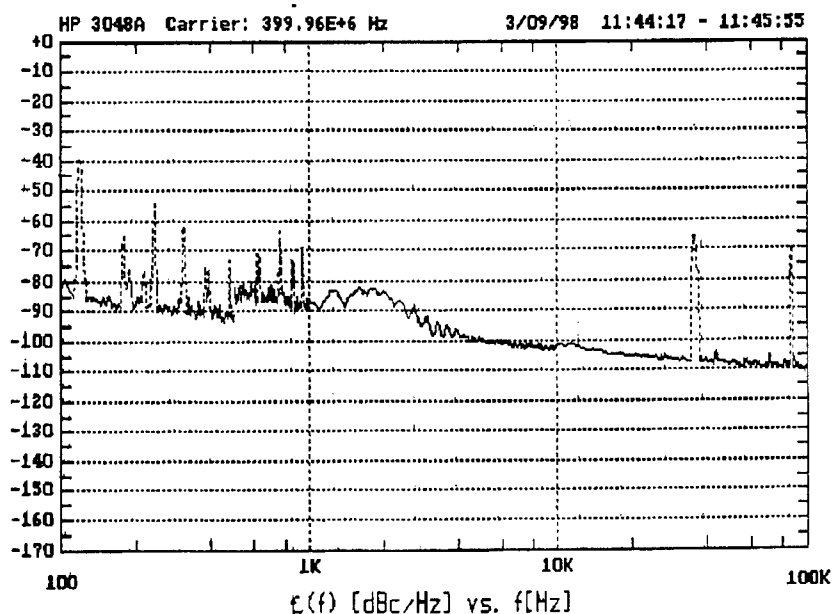


Figure 19: Single-sideband phase noise of photonic synthesizer operated at 10 GHz. The HP3048A phase noise test system was used to downconvert the 10 GHz signal to 400 MHz by using the HP70427A microwave downconverter.

carrier as measured using the HP3048A phase noise measurement system. In Fig.20, the phase noise of the Photonic Synthesizer is plotted at several frequencies from 1 GHz to 50 GHz at 10 kHz offset from the carrier. For comparison, the phase noise of a Hewlett-Packard HP83650L 10 MHz - 50 GHz microwave synthesizer was also measured and is plotted. Table-2 gives a summary of these results. These results show that the Photonic Synthesizer phase noise is about 14 dB to 20 dB lower than a high-quality commercially-available RF wide-frequency-range synthesizer such as the HP83650L over the frequency range of 10 GHz to 50 GHz. These results were obtained using the fiber ring mode locked laser as the optical comb generator.

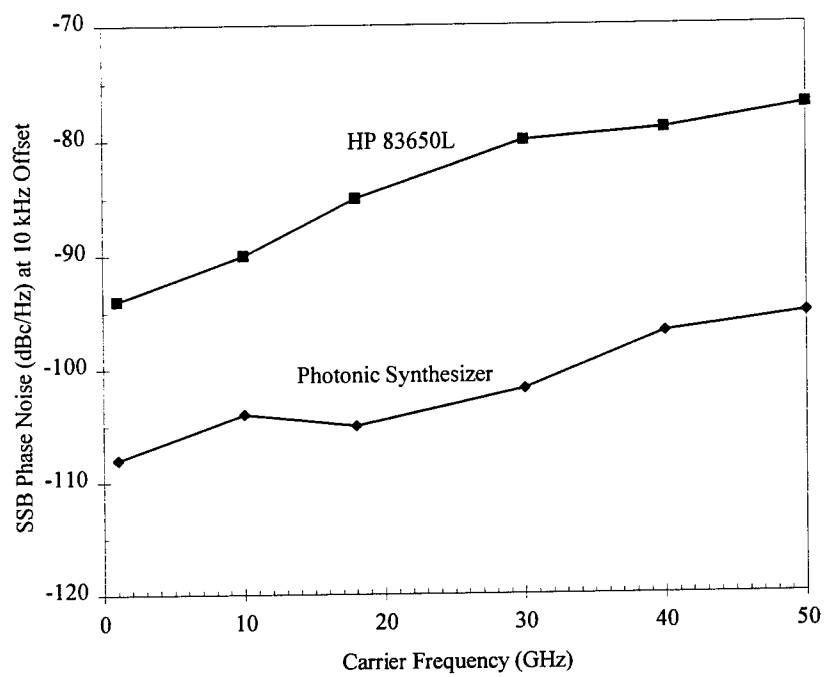


Figure 20: Single-sideband phase noise of photonic synthesizer and HP83650L at frequency offset of 10 kHz.

Table-2: Summary of Phase Noise Results		
SSB Phase Noise PSD [dBc/Hz] at 10 kHz offset		
Frequency (GHz)	Photonic Synthesizer	HP 83650L
1	-108	-94
10	-104	-90
18	-105	-85
30	-102	-80
40	-97	-79
50	-95	-77

4 Theoretical Model

4.1 Introduction to injection-locking of semiconductor lasers

In this Section, a theoretical model for the Photonic Synthesizer is developed. The model starts from a treatment of injection locking in semiconductor lasers, then proceeds to an analysis of the phase noise of the detected RF heterodyne beat.

Injection locking is a way of synchronizing one (or several) free-running oscillators to a reference oscillator. The technique was described in the classic papers of van der Pol [17] and Adler [18] for the case of electrical oscillators, and injection locking of microwave oscillators was reported by Kurokawa. Injection locking of lasers has been extensively investigated both theoretically and experimentally. Initially, it was studied on the basis of the general theory of injection locking in regenerative oscillators [21] - [24]. Later, an injection-locking theory based on semiconductor rate equations was developed by Lang [25] and several others [26, 27].

An early motivation to study injection locking in semiconductor lasers was for application in long-distance high-speed digital fiber-optic transmission systems. It was found that injection locking reduced the spectral broadening during high speed modulation which limits the transmission distance due to fiber dispersion. For coherent transmission systems, injection locking may be used to synchronize the local oscillator. It can also be used to generate phase shift keying (PSK) modulation and to provide homodyne detection with optimum receiver sensitivity. Pulsations induced by optical injection have also been found to yield information about the important coupling between amplitude and phase of the electric field in a semiconductor laser. In fact, a method was developed to measure the laser linewidth enhancement factor α using injection locking techniques [29].

Previously, it was widely known that injection-locking of semiconductor lasers can create instabilities and even chaos when injection power increased beyond a certain critical level. Therefore, the operation of the injection-locked laser was kept under this instability boundary to ensure stable operation. However, this also limits the locking bandwidth to a rather small range, which leads to a relatively small modulation bandwidth. Recently, it was discovered that when a laser is operated under very strong injection-locking conditions, which were not analyzed previously, the laser instability disappears and a stable operation region emerges. Under this strong injection-locking condition, several groups found enhancement of laser direct modulation bandwidth compared to the free-running situation, and

reduced chirp [31] - [35]. These discoveries may result in renewed interest in injection-locking techniques for fiber communication applications. Also, injection-locking to a sideband of a modulated laser to generate high frequency microwave signals has recently been proposed and demonstrated [10, 15]. It has also recently been demonstrated that high frequency millimeter wave signals to 64 GHz can be generated through injection-locking [30], for application in mobile communications systems.

4.2 Analysis of DFB laser injection-locking

In this section, we will review the theory of the injection-locked semiconductor laser. We will derive some important parameters regarding the injection-locking frequency range, injection power ratio, and stability of injection locking.

In the DFB semiconductor lasers used in the Photonic Synthesizer, the longitudinal modes other than the main mode (i.e., side-modes) are highly suppressed and dynamic single mode operation is ensured by the mechanism of distributed feedback. We thus use the well-known single-mode rate equations for the laser field and carrier density [25] - [27]. We develop rate equations for the slave laser receiving the injected field from the master laser. We assume there is no injection from the slave laser back to the master laser.

The DFB semiconductor laser with an external optical injection field can be described as

$$\frac{dP}{dt} = [\Gamma G_N(N - N_0) - \frac{1}{\tau_p}]P + \frac{c}{Ln} \sqrt{\eta P P_i} \cos \theta, \quad (1)$$

$$\frac{d\phi}{dt} = -\Delta\omega + \frac{1}{2}\alpha\Gamma G_N(N - N_{th}) + \frac{c}{2Ln} \sqrt{\frac{\eta P_i}{P}} \sin \theta, \quad (2)$$

$$\frac{dN}{dt} = \frac{J}{eV} - \frac{N}{\tau_e} - G_N(N - N_0)P/V, \quad (3)$$

where the electric field of the slave laser is defined as

$$E = \sqrt{P} e^{j(\omega_i t + \phi)} \quad (4)$$

and the master laser injection electric field is

$$E_i = \sqrt{P_i} e^{j(\omega_i t + \phi_i)}. \quad (5)$$

Other parameters are:

P : photon number of the slave laser,

P_i : photon number of the master (injection) laser,

ϕ : phase of the electric field for the slave laser,
 ϕ_i : phase of the electric field for the master laser,
 $\theta = \phi_i - \phi$: phase difference between the master laser and the slave laser,
 $\Delta\omega = \omega_i - \omega$: detuning between the master laser and the free-running slave laser,
 N : carrier density,
 N_0 : carrier density at transparency,
 N_{th} : carrier density at threshold,
 $G = G_N(N - N_0)$: material gain,
 G_N : differential gain,
 Γ : confinement factor,
 τ_p : photon lifetime,
 α : linewidth enhancement factor,
 L : laser cavity length,
 $\frac{c}{n}$: group velocity,
 τ_e : carrier lifetime,
 V : active volume,
 J : injection current,
 η : coupling coefficient of the master laser to the slave laser.

We first seek the steady state solution of the system of equations Eq.(1)-Eq.(3) which yields important information such as the conditions for stable locking. From Eq.(1), setting $dP/dt = 0$, we have

$$[\Gamma G_N(N - N_0) - \frac{1}{\tau_p}]P + \frac{c}{Ln} \sqrt{\eta P P_i} \cos \theta = 0. \quad (6)$$

Using the relation at laser threshold

$$\frac{1}{\tau_p} = \Gamma G_N(N_{th} - N_0), \quad (7)$$

we obtain from Eq.(6)

$$\Gamma G_N(N - N_{th}) = -\frac{c}{Ln} \sqrt{\frac{\eta P_i}{P}} \cos \theta. \quad (8)$$

Substituting Eq.(8) into the phase equation Eq.(2), we obtain the new phase equation as

$$\frac{d\phi}{dt} = -\Delta\omega + \frac{c}{2Ln} \sqrt{\frac{\eta P_i}{P}} (\sin \theta - \alpha \cos \theta). \quad (9)$$

We then define two new parameters as

$$K = \frac{c}{2Ln} \sqrt{\frac{\eta P_i}{P}} \sqrt{1 + \alpha^2}, \quad (10)$$

$$\theta_0 = \arctan \alpha. \quad (11)$$

We can then rewrite Eq.(9) using these two parameters as

$$\frac{d\phi}{dt} = -\Delta\omega + K \sin(\theta - \theta_0). \quad (12)$$

Eq.(12) is the well-known Adler's equation which describes injection locking of two oscillators [18]. When the two lasers are free-running their frequency detuning satisfies the condition

$$-K \leq \Delta\omega \leq K. \quad (13)$$

The phase Eq.(12) has the stationary solution of

$$\theta = \theta_0 + \arcsin \frac{\Delta\omega}{K} + q2\pi \quad (14)$$

where q is an integer. Eq.(12) has another stationary solution

$$\theta = \theta_0 + \pi - \arcsin \frac{\Delta\omega}{K} + q2\pi, \quad (15)$$

however, this solution is not stable since it yields $\cos(\theta - \theta_0) < 0$. So we only consider the stable solution given by Eq.(14).

The condition given by Eq.(13) is the so-called injection-locking condition: for a given injection power, it determines the maximum detuning for locking of the master and slave lasers. We rewrite the locking condition of Eq.(13) by replacing parameter K with the original laser cavity parameters as given in Eq.(10)

$$|\Delta\omega| \leq \frac{c}{2Ln} \sqrt{\frac{\eta P_i}{P}} \sqrt{1 + \alpha^2}. \quad (16)$$

We shall call the maximum detuning the locking bandwidth. Fig.21 displays an example of the locking bandwidth as a function of the ratio of injection power to the slave laser vs. its output power. The above locking condition defines the boundary of the frequency detuning for the injection locking. All the points inside the two curves given by $|\Delta\omega| = \frac{c}{2Ln} \sqrt{\frac{\eta P_i}{P}} \sqrt{1 + \alpha^2}$ are stationary solutions, which means any detuning value falling inside this

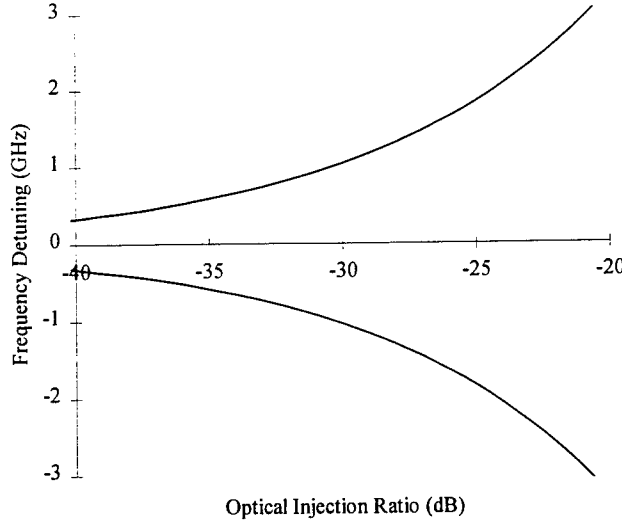


Figure 21: Locking range as a function of the injection power to DFB slave laser output power ratio, P_i/P (dB). When the frequency detuning value $\Delta\omega$ is inside the area defined by these two curves, the slave laser phase can lock to the master laser phase.

range will guarantee locking of the slave laser phase to the master laser. For detuning values lying outside the two curves, the slave laser phase can not lock to the master laser phase. As we see from the locking condition, the locking range increases as the injection level increases. However, as will be shown in the following stability analysis, the stationary solution is unconditionally stable only when the injection level is smaller than a certain threshold level.

We use the following parameters, which approximate the DFB slave lasers used in our experiments, to produce the theoretical calculations used in Fig.21 and throughout the remainder of this analysis: DFB laser cavity mode spacing $\frac{c}{2Ln} = 40$ GHz, linewidth enhancement factor $\alpha = 5$, injection coupling ratio $\eta = 2.6\%$. These parameters yield the overall parameter $\frac{c}{2Ln}\sqrt{\eta(1+\alpha^2)} = 33$ GHz which is used in Eq.(16) to produce the curves in Fig.21.

4.3 Stability analysis of injection-locked lasers

Instabilities in the injection-locking of lasers have been studied extensively. It was found that the steady-state condition discussed in the previous section can become unstable when the injection level increases beyond a certain level. Since injection-locking as described by Eq.(1-3) is a nonlinear dynamical system with three variables, many interesting phenomena such as Hopf-bifurcation, period-doubling, and chaos have been observed in this system [36, 37]. However, in this work we are concerned with maintaining stable injection-locking, so we next perform a thorough investigation of the parameter space with a goal of maximizing the set of stable solutions.

Following the standard method to analyze the stability of the steady-state solution, we define a small perturbation around the stationary-state values of the photon number, carrier density, and phase:

$$P(t) = P + \delta P(t), \quad (17)$$

$$N(t) = N + \delta N(t), \quad (18)$$

$$\phi(t) = \phi + \delta\phi(t). \quad (19)$$

We then use these definitions to linearize equations Eq.(1-3)

$$\frac{d\delta P(t)}{dt} = -\rho \cos \theta \delta P(t) + 2\rho P \sin \theta \delta\phi(t) + \Gamma G_N P \delta N(t), \quad (20)$$

$$\frac{d\delta\phi(t)}{dt} = -\frac{\rho \sin \theta}{2P} \delta P(t) - \rho \cos \theta \delta\phi(t) + \frac{1}{2} \alpha \Gamma G_N \delta N(t), \quad (21)$$

$$\frac{d\delta N(t)}{dt} = -\frac{G}{V} \delta P(t) - \frac{1}{\tau_R} \delta N(t), \quad (22)$$

where we have defined two new parameters

$$\rho = \frac{c}{2Ln} \sqrt{\frac{\eta P_i}{P}}, \quad (23)$$

$$\frac{1}{\tau_R} = \frac{1}{\tau_e} + \frac{G_N P}{V}. \quad (24)$$

The parameter ρ is the so-called normalized optical injection level, which has units of frequency; τ_R is the damping time of the relaxation oscillation for the free-running DFB laser diode.

The eigenvalues λ of the above linear equations satisfy the relation

$$\det \begin{pmatrix} -\lambda - \rho \cos \theta & 2\rho P \sin \theta & \Gamma G_N P \\ -\frac{\rho \sin \theta}{2P} & -\lambda - \rho \cos \theta & \frac{1}{2} \alpha \Gamma G_N \\ -\frac{G}{V} & 0 & -\lambda - \frac{1}{\tau_R} \end{pmatrix} = 0 \quad (25)$$

This leads to a cubic algebraic equation for the eigenvalue λ

$$\lambda^3 + a_2\lambda^2 + a_1\lambda + a_0 = 0, \quad (26)$$

where the coefficients are

$$a_2 = \frac{1}{\tau_R} + 2\rho \cos \theta, \quad (27)$$

$$a_1 = \rho^2 + \frac{2\rho}{\tau_R} \cos \theta + \omega_R^2, \quad (28)$$

$$a_0 = \frac{\rho^2}{\tau_R} + \rho\omega_R^2(\alpha \sin \theta + \cos \theta), \quad (29)$$

and the parameter

$$\omega_R = \sqrt{\frac{G_N P}{V\tau_p}} \quad (30)$$

is the relaxation frequency of the slave laser.

For the weak injection level as in the case of our experiments, the injection-locked state becomes unstable when the damping rate of the relaxation oscillation at approximately frequency ω_R becomes zero. This corresponds to the situation where the eigenvalue λ crosses the imaginary axis in the complex plane. At the instability boundary, the eigenvalue becomes a pure imaginary number

$$\lambda_{1,2} \simeq \pm j\omega_R, \quad (31)$$

where we have used the condition $\omega_R \gg \rho$, which is valid under the assumption of weak injection level. In our experiment, the typical value of ω_R is around 6-10 GHz, while the value of ρ is less than 0.7 GHz.

Substituting Eq.(31) into the eigenvalue equation Eq.(26), we obtain the stability boundary as given by

$$\frac{1}{\tau_R} = \rho(\alpha \sin \theta - \cos \theta). \quad (32)$$

Using the definition given by Eq.(10-11), Eq.(32) can be rewritten as

$$\frac{1}{\tau_R} = -K \cos(\theta + \theta_0). \quad (33)$$

Eq.(33) shows that if

$$K < \frac{1}{\tau_R}, \quad (34)$$

there is no solution that satisfies Eq.(33), which means that under this condition the injection locking solution is unconditionally stable. Eq.(34) thus sets an upper limit for the injection level; as long as the injection level is smaller than this level, the injection locking is always stable.

On the other hand, when the injection level approaches the level such that

$$K > \frac{1}{\tau_R}, \quad (35)$$

we have instabilities, since there can be no solutions of phase that satisfy Eq.(33). However, even under these conditions, there are steady states which do not meet Eq.(33) but are still stable. A range of values inside the boundary of the steady state as shown in Fig.21 become unstable, while a small set of values still stable. The boundary defining this range can be calculated from Eq.(33). In fact, we obtain from Eq.(33)

$$\theta = \pi - \arccos\left(\frac{1}{\tau_R K}\right) - \theta_0, \text{ and} \quad (36)$$

$$\theta = \pi + \arccos\left(\frac{1}{\tau_R K}\right) - \theta_0, \quad (37)$$

and from Eq.(12) the detuning is given as

$$\Delta\omega = K \sin(\theta - \theta_0). \quad (38)$$

Substituting Eq.(36,37) into Eq.(38), we obtain the two instability boundaries

$$\Delta\omega = K \sin[2\theta_0 + \arccos\left(\frac{1}{\tau_R K}\right)], \text{ and} \quad (39)$$

$$\Delta\omega = K \sin[2\theta_0 - \arccos\left(\frac{1}{\tau_R K}\right)]. \quad (40)$$

In Fig.22, we plot the instability boundaries given by Eq.(39,40). We chose typical parameters for our semiconductor laser to have carrier lifetime $\tau_e = 2 \times 10^{-9}$ s and photon life time $\tau_p = 2 \times 10^{-12}$ s; other parameters are the same as used in the previous calculations plotted in Fig.21. We assume a value of the relaxation oscillation frequency of 6 GHz which is within the range measured for our laser. This yields a damping rate of $\frac{1}{\tau_R} = 3.3$ GHz. From Fig.22, we can see that as long as the injection level ratio is lower than about -20 dB, the locking solution is always stable. However, at high injection levels, a large portion of the area within the locking range boundary

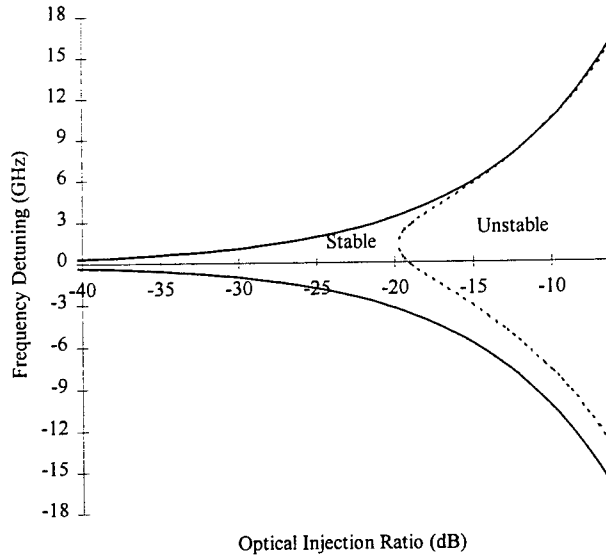


Figure 22: Stable and unstable injection-locking range as a function of injection power level. The area inside the lines is the stable region.

becomes unstable. An interesting feature of this plot is that the unstable area is asymmetric with respect to the detuning. Almost all the positive detuning is unstable for large injection levels, while a portion of negative detuning close to the locking boundary remains stable. There are essentially no practical consequences of this instability region for the operation of the Photonic Synthesizer, since the injection locking range must be kept less than the mode-locked laser mode spacing of 1 GHz, which occurs at optical injection ratios less than -20 dB.

4.4 Experimental confirmation of injection-locking analysis

Experiments were performed to confirm the theoretical predictions of the locking range as a function of injection power and frequency detuning for our CW DFB lasers using the setup illustrated in Fig.23. Both the master laser and slave laser are DFB lasers operated as CW sources. These are the same type of lasers used as the slave lasers in the Photonic Synthesizer. The master laser is injected into the slave laser through a 10/90 fiber-optic

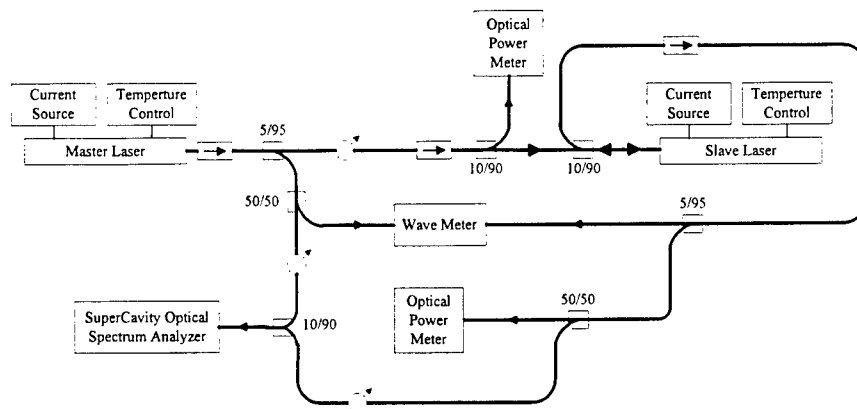


Figure 23: Experimental setup used to measure the injection locking frequency range as a function of injection power level for two CW DFB lasers.

coupler. Two optical isolators with isolation of more than 50 dB each are used to prevent any coupling back from the slave laser to the master laser. An optical power meter is used to measure the master laser injection level through a second 10/90 fiber-optic coupler.

A high-accuracy wavemeter was used to measure the absolute frequency of the optical output from both lasers. The wavemeter accuracy is ± 0.0001 nm or ± 0.03 GHz with ± 0.01 GHz resolution. Both outputs from the slave laser and master laser were combined with a fiber-optic coupler and displayed simultaneously using a Newport Supercavity optical spectrum analyzer to observe the locked and unlocked states. To determine the locking range, we first adjusted the slave laser frequency to be within the locking range, such that the slave laser become locked to the master laser. This is accomplished by adjusting the laser temperature and current. After the slave laser is locked to the master laser, we carefully changed the slave laser current until the slave laser unlocked from the master laser, which was observed as a sharp jump of the slave laser frequency. We then measured the frequency difference between the master laser and the free-running slave laser with the wavemeter. This value is the detuning at the locking boundary for a given injection level. The same procedure was repeated at several different injection power levels for both positive and negative frequency detuning.

Fig.24 summarizes the experimental results for the locking range as a function of the injection level. To generate the theoretical fit, we used the same parameters as in Fig.21. They are: DFB laser cavity mode spacing

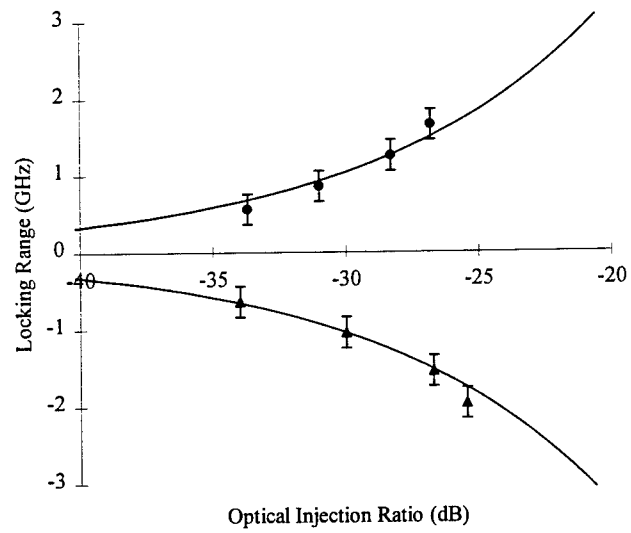


Figure 24: Experimental data and theoretical fit for the locking frequency range as a function of injection power level.

$\frac{c}{2Ln} = 40$ GHz, linewidth enhancement factor $\alpha = 5$. These values closely match the DFB lasers used in the experiments and they are used throughout this report for all theoretical calculations. However, it is difficult to estimate the coupling ratio from the injection master laser to the slave laser, and it is the only parameter we need to adjust in order to fit the experimental data. In this case, a coupling ratio of $\eta = 2.6\%$ yields the best fit to the experimental data.

As we further increase the injection power to the slave laser, we observe the excitation of the oscillation at relaxation frequency ω_R . This can be observed using the Supercavity optical spectrum analyzer, as Fig.25 shows there are two smaller symmetric modulation peaks that appear in the slave laser optical spectrum. To verify that these two modulation peaks are indeed at the relaxation frequency as Eq.(31) predicts, we measure the frequencies of these oscillations for different slave laser output power levels. The laser relaxation frequency is proportional to the square root of the laser output power as shown in Eq.(30). We therefore should be able to fit the measured slave laser modulation frequency when it is in the instability zone as Fig.25(c) shows. Fig. 26 displays the measured modulation frequency and the theoretical fitting using the relation derived from Eq.(30)

$$f_R = b\sqrt{P}, \quad (41)$$

where b is the fitting parameter used in the figure, P is the optical output power in mW, $f_R = \omega_R/2\pi$ is the relaxation frequency in GHz. From the figure we see that the data falls within $\pm 5\%$ from the best fitting parameter $b = 0.99$. This confirms the oscillation we observe is indeed the relaxation frequency as we analyzed in the previous section.

4.5 Phase noise analysis of injection-locked lasers

Phase noise of injection-locked lasers has been the subject of intensive previous study [20, 21, 22, 23, 24, 25, 26, 27, 28, 29]. It was found that the slave laser phase follows only the phase fluctuations of the master laser, so the slave laser linewidth will be equal to the linewidth of the master laser, independent of the output power of the slave laser. In this section, we present a review and detailed discussion of the phase noise of injection-locked semiconductor lasers. This will form the theoretical basis for understanding the phase noise of the heterodyne output of the Photonic Synthesizer.

The small phase fluctuations of the slave laser and the master laser are defined as $\delta\phi(t)$ and $\delta\phi_i(t)$ respectively, and are assumed to be much less

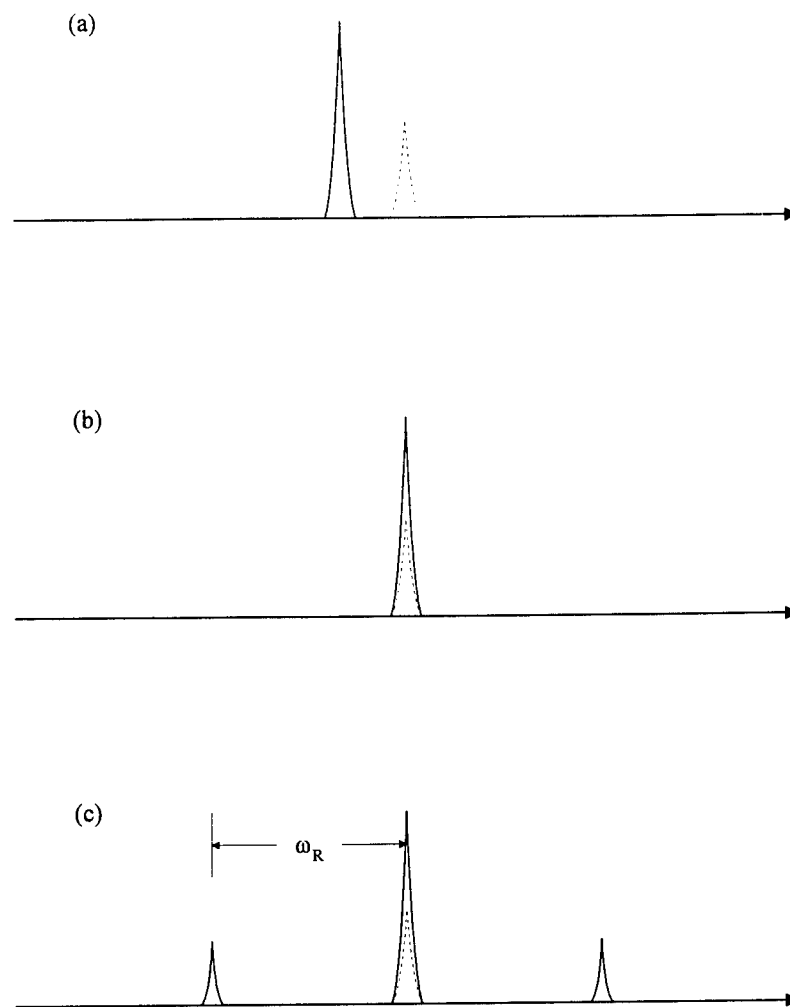


Figure 25: Illustration of optical spectrum analyzer display during the injection-locking experiments. The solid line is the slave laser; the dashed line is the master laser. (a). The slave laser is in the free-running condition with no injection from the master laser. There is a small amount of detuning between the frequency of the master laser and the slave laser. (b). The slave laser frequency is locked to the master laser with low injection level, so the slave laser is stable. (c). Further increasing the injection level, the slave laser is driven into the instability zone. Two side modes at the relaxation oscillation frequency are developed due to the excitation of the oscillation by the high injection level.

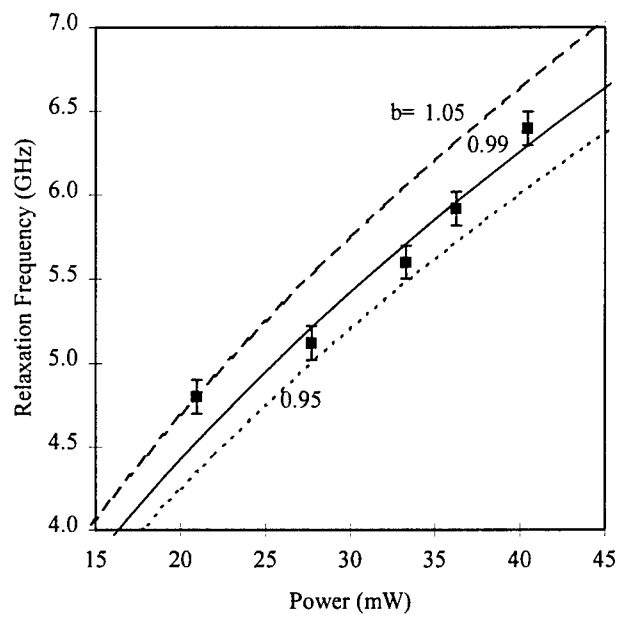


Figure 26: Measured oscillation frequency as a function of slave laser output power. The solid line is the best fit; the long dash and short dash lines are the fitting with parameters $\pm 5\%$ different from the best fitting parameter.

than one cycle of phase. We can obtain the equations for phase fluctuations by linearizing the phase equation (12) around the stationary solution,

$$\frac{d\delta\phi(t)}{dt} = K \cos(\theta - \theta_0)[\delta\phi_i(t) - \delta\phi(t)] + F(t). \quad (42)$$

We omit the noise terms due to the slave and master laser relative intensity noise (RIN) contributions to the phase fluctuation in Eq.(42), since they are much smaller than the phase noise contribution from the master laser, and the slave laser spontaneous emission noise term, $F(t)$. The spontaneous emission noise of the slave laser, $F(t)$, is related to the laser quantum Langevin noise sources from the semi-classical model of the semiconductor laser as

$$F(t) = F_\phi(t) + \frac{\alpha}{2P} F_p(t). \quad (43)$$

$F_p(t)$ and $F_\phi(t)$ are the Langevin noise sources for the laser intensity and phase respectively. They are independent Markov process satisfying

$$\langle F_p(t) F_p(t - \tau) \rangle = 2RP\delta(\tau), \quad (44)$$

$$\langle F_\phi(t) F_\phi(t - \tau) \rangle = \frac{R}{2P} \delta(\tau), \quad (45)$$

where $R = \frac{n_{sp}}{\tau_p}$ is the spontaneous emission rate; n_{sp} is the so-called inversion factor while τ_p is the photon lifetime. Eq.(43) shows that due to the linewidth enhancement factor α , the laser intensity fluctuation noise source $F_p(t)$ is coupled to the total laser phase noise source $F(t)$.

Before we analyze the phase noise of the injection-locked laser, we first briefly discuss the phase noise of the free-running laser, and calculate the laser linewidth. The phase fluctuations of the free-running laser without injection are given by eliminating the injection term in Eq.(42), which yields

$$\frac{d\delta\phi(t)}{dt} = F(t). \quad (46)$$

The Fourier transform of the above equation is

$$\delta\phi(f) = \frac{F(f)}{j2\pi f}. \quad (47)$$

The power spectrum of the phase noise is thus given by

$$S_{\delta\phi}(f) = \frac{\Delta\nu}{2\pi f^2}, \quad (48)$$

where $\Delta\nu$ is the laser linewidth. It is calculated as

$$\Delta\nu = \frac{R}{4\pi P}(1 + \alpha^2), \quad (49)$$

where we used Eq.(44,45) to obtain $\Delta\nu$. The laser linewidth $\Delta\nu$ is inversely proportional to the laser output power. The semiconductor laser linewidth enhancement factor α broadens the laser linewidth considerably. The power spectrum is Lorentzian with a pole at Fourier frequency $f = 0$.

We now return to the phase noise of the injection-locked laser. We define a new parameter as

$$\Omega = K \cos(\theta - \theta_0). \quad (50)$$

For the stationary state, we have from Eq.(12) the relation

$$\Delta\omega = K \sin(\theta - \theta_0). \quad (51)$$

Therefore, we obtain

$$\cos(\theta - \theta_0) = \frac{\sqrt{K^2 - \Delta\omega^2}}{K}, \quad (52)$$

and

$$\Omega = \sqrt{K^2 - \Delta\omega^2}. \quad (53)$$

From Eq.(42), we obtain the Fourier transform of the phase fluctuation

$$\delta\phi(f) = \frac{\Omega}{\Omega + j2\pi f} \delta\phi_i(f) + \frac{F(f)}{\Omega + j2\pi f}. \quad (54)$$

The phase noise power spectrum in the injection locked condition is thus given by

$$S_{\delta\phi}(f) = \frac{\Omega^2}{\Omega^2 + 4\pi^2 f^2} S_{\delta\phi_i}(f) + \frac{2\pi\Delta\nu}{\Omega^2 + 4\pi^2 f^2}. \quad (55)$$

Since the master laser is free-running, its phase noise power spectrum is given by Eq.(48)

$$S_{\delta\phi}(f) = \frac{\Delta\nu_i}{2\pi f^2}, \quad (56)$$

where $\Delta\nu_i$ is the linewidth of the free-running master laser.

Therefore, the optical phase noise power spectrum for the injection-locked laser becomes

$$S_{\delta\phi}(f) = \frac{\Omega^2}{\Omega^2 + 4\pi^2 f^2} \frac{\Delta\nu_i}{2\pi f^2} + \frac{2\pi\Delta\nu}{\Omega^2 + 4\pi^2 f^2}. \quad (57)$$

The power spectrum has a pole at zero frequency from the master laser, which becomes the dominant term for the injection-locked laser. This result indicates that the slave laser phase will follow the master laser phase fluctuations in the injection-locked condition. In fact, Eq.(57) gives the same linewidth as the master laser [16].

4.6 Residual phase noise of the Photonic Synthesizer

Applying the results developed in the previous section for the phase noise of the injection-locked lasers, we may now analyze the phase noise of the Photonic Synthesizer.

We first examine the phase noise of the mode-locked laser. We are interested in the correlation of the phase fluctuations of the individual modes of the mode-locked laser. Assuming the phase fluctuation of the RF source that drives the mode-locked laser is given by $\delta\phi_R$, the phase noise of any two longitudinal modes numbered i and k of the mode-locked laser can be written as

$$\delta\phi_i = \delta\phi_0 + i\delta\phi_R, \quad (58)$$

$$\delta\phi_k = \delta\phi_0 + k\delta\phi_R. \quad (59)$$

Mode i and mode j are separated from each other in the frequency domain by $(k - j)f_R = mf_R$, where f_R is the frequency of the RF driving source. $\delta\phi_0$ is the common phase fluctuation for all modes of the mode-locked laser due to spontaneous emission noise, similar to the single-mode free-running laser case. We assume $\delta\phi_0$ is the same for all modes of the mode-locked laser, which turns out to be a reasonable assumption. The value of $\delta\phi_0$ is generally much larger than the RF phase noise $\delta\phi_R$, since the linewidth of the laser is typically on the order of 1 MHz, while the linewidth of the RF oscillator is on the order of 0.001 Hz or less. In the Photonic Synthesizer, mode i and mode j are filtered out using the injection-locking technique or some other very narrow optical filtering technique and their photodetected beat generates an RF signal at frequency of mf_R . Assuming that there are no large optical path-length differences for the two modes, we expect that the phase noise $\delta\phi_0$ common to the two modes will cancel out, resulting

in a high-quality RF signal with phase noise determined largely by the RF driving oscillator, but with some added noise due to the injection-locking process.

In the injection-locked case, the whole comb of the mode-locked laser is injected into the two CW DFB lasers. Suppose DFB laser #1 is locked to mode i , DFB laser #2 is locked to mode k . Then, using the results from the previous section and Eq.(54), we obtain the phase noise for laser #1 and laser #2 as

$$\delta\phi_1(f) = \frac{\Omega_1}{\Omega_1 + j2\pi f}(\delta\phi_0 + i\delta\phi_R) + \frac{F_1(f)}{\Omega_1 + j2\pi f}, \quad (60)$$

$$\delta\phi_2(f) = \frac{\Omega_2}{\Omega_2 + j2\pi f}(\delta\phi_0 + k\delta\phi_R) + \frac{F_2(f)}{\Omega_2 + j2\pi f}. \quad (61)$$

The locking bandwidths in our injection-locking experiments are in the range of several hundred MHz to 1 GHz. We adjust the detuning to be less than 100 MHz, so that Ω_1 and Ω_2 are in the range of several hundred MHz as well. We are interested in the resulting photodetected RF signal phase noise at frequency offsets from the RF carrier of 100 Hz to 100 kHz. Therefore we have $\Omega_1, \Omega_2 \gg 2\pi f$. We thus can approximate Eq.(60-61) as

$$\delta\phi_1(f) = \delta\phi_0(f) + i\delta\phi_R(f) + \frac{F_1(f)}{\Omega_1 + j2\pi f}, \quad (62)$$

$$\delta\phi_2(f) = \delta\phi_0(f) + k\delta\phi_R(f) + \frac{F_2(f)}{\Omega_2 + j2\pi f}. \quad (63)$$

The phase noise of the resulting RF signal at frequency of mf_R due to the heterodyne photodetection of laser #1 and laser #2 is given by

$$\delta\phi_{21}(f) = \delta\phi_2(f) - \delta\phi_1(f) = m\delta\phi_R(f) + \frac{F_1(f)}{\Omega_1 + j2\pi f} + \frac{F_2(f)}{\Omega_2 + j2\pi f}. \quad (64)$$

For simplicity, we assume both DFB lasers have the same locking bandwidth and detuning, so $\Omega_1 = \Omega_2$. We also assume both lasers have the same linewidth $\Delta\nu$. In this case, the phase noise power spectrum of the Photonic Synthesizer output is

$$S_{\delta\phi_{21}}(f) = m^2 S_R(f) + \frac{4\pi\Delta\nu}{\Omega^2}. \quad (65)$$

$S_R(f)$ is the phase noise power spectrum for the RF source that drives the mode-locked laser. The first term in Eq.(65) is the multiplied phase noise of the RF source. Because the output RF signal frequency is m times the

fundamental frequency f_R of the RF source, this phase noise follows the rule of $20 \log(m)$. The last term of Eq.(65) represents the added noise or residual phase noise of the Photonic Synthesizer due to the injection-locking process. It is a function of Ω which depends on locking range and detuning. This last term depends linearly on the slave laser linewidth $\Delta\nu$, where we have assumed that both slave lasers have the same instantaneous linewidth. We note that this analysis neglects any residual phase noise added by the mode-locked laser. This is equivalent to our assumption that the only noise source in the mode-locked laser is spontaneous emission noise that is common to all modes. If the actively mode-locked laser is well designed with minimum detuning, its contribution to the RF phase noise is smaller than the RF driving source for most cases [11]. However, if the laser is incompletely mode-locked, or if other technical noise sources cause perturbations of the phases of the individual modes, then the phase noise could be degraded beyond the result of Eq.(65).

The *residual* phase noise of the Photonic Synthesizer is defined as the noise contribution above the multiplied reference oscillator phase noise. It is given by

$$S_{res}(f) = \frac{4\pi\Delta\nu}{\Omega^2} = \frac{4\pi\Delta\nu}{K^2 - \Delta\omega^2}. \quad (66)$$

Here we have explicitly replaced Ω^2 using the locking range K^2 and detuning $\Delta\omega^2$. We note that $S_{res}(f)$ is constant versus frequency offset f , since we have assumed that Ω is on the order or several hundred MHz. In Fig.27, we plot the $S_{res}(f)$ as function of the locking range K assuming detuning $\Delta\omega = 0$ for two different slave laser intrinsic linewidths $\Delta\nu$ of 100 kHz and 1 MHz. From Fig.27, we see that the residual phase noise decreases as the locking range increases. However, in our case we can not increase the locking range beyond 500 MHz, or other modes will introduce large sidebands in the resulting RF signal. The residual phase noise also decreases as the slave laser linewidth decreases. This motivates the choice of narrow-linewidth lasers to achieve the lowest residual phase noise.

In Fig.28, we plot the residual phase noise of the Photonic Synthesizer as a function of the detuning for locking ranges of 500 MHz and 1000 MHz. We use a slave laser linewidth of 1 MHz in these calculations. The residual phase noise decreases with smaller detuning. When the detuning value approaches the locking range, the residual phase noise increases very rapidly. In order to obtain the minimum residual phase noise in practice, the slave laser frequencies must be adjusted so that the detuning is minimized. How-

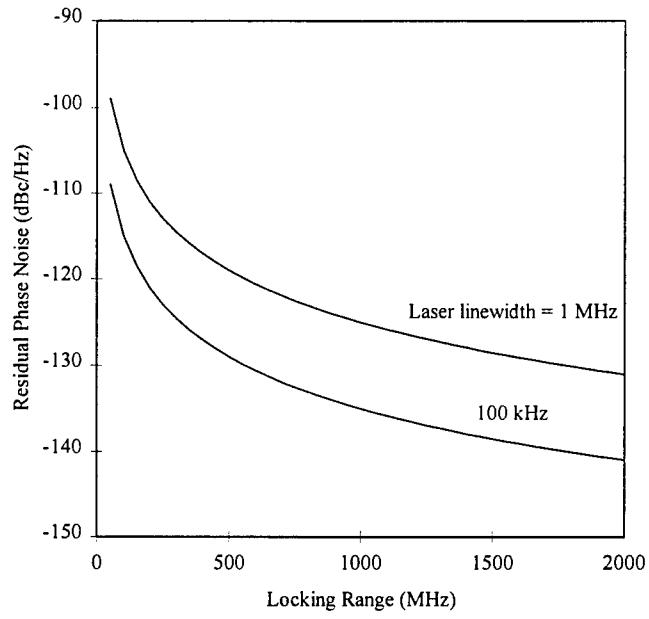


Figure 27: Photonic synthesizer residual phase noise $S_{res}(f)$ as a function of the locking range K . We assume the master-slave laser detuning $\Delta\omega = 0$; the calculation is performed for the cases of slave laser intrinsic linewidth of 100 kHz and 1 MHz.

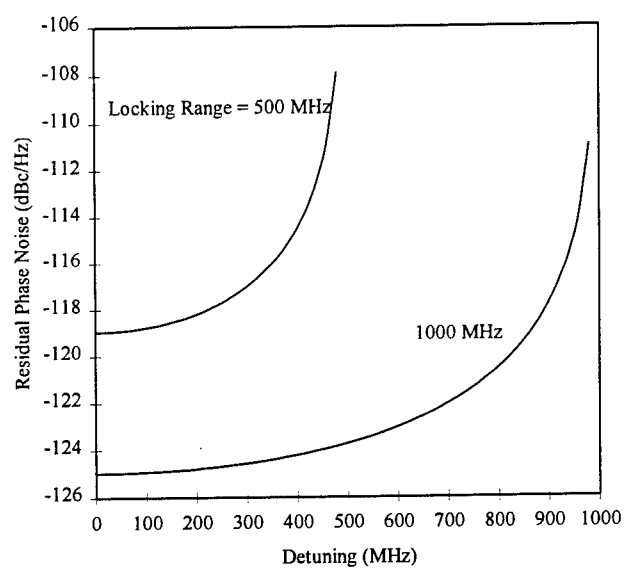


Figure 28: Photonic synthesizer residual phase noise as a function of the detuning $\Delta\omega$ for locking range K of 500 MHz and 1000 MHz. We assume the slave laser linewidths are 1 MHz.

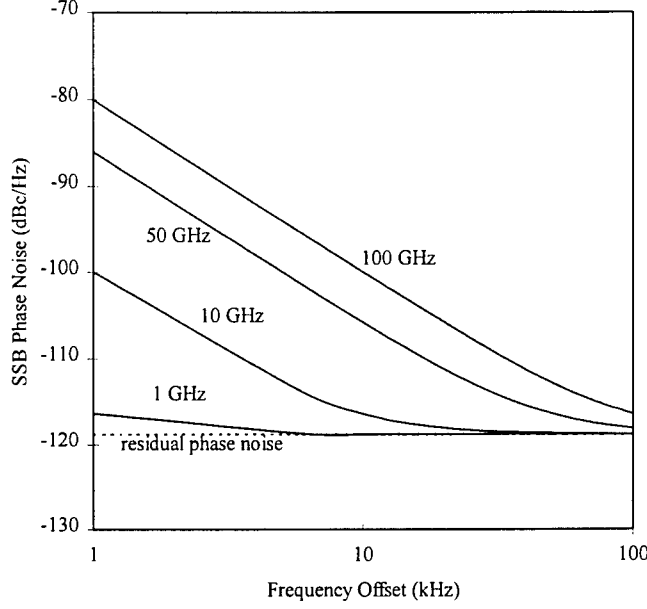


Figure 29: Calculated SSB phase noise of the Photonic Synthesizer from Eq.(65). We assume the RF source follows the ideal $-20 \log(f)$ rule for its close-to-carrier phase noise and has -120 dBc/Hz at 1 kHz offset. We also assume 1 MHz slave laser linewidths, 500 MHz locking range, and 100 MHz detuning. The dashed line is the residual phase noise represented by the second term in Eq.(65), which sets the lowest limit for the achievable phase noise for the assumed parameters.

ever, it is fortuitous that the residual phase noise level is not a very strong function of detuning. In fact, the phase noise level changes only 1.5 dB for values in the range of zero detuning to detuning of 70% of the locking range. These considerations define the requirements on the tuning accuracy of the slave lasers to achieve a given level of performance.

Finally, we plot the theoretical estimation of the single side-band (SSB) phase noise for the Photonic Synthesizer in Fig.29. For the purposes of the calculation, we model the 1 GHz RF source phase noise as

$$S_R(f) = \frac{\Delta\nu_R}{2\pi f^2}, \quad (67)$$

where we use $\Delta\nu_R = 6.28 \mu\text{Hz}$ which results in SSB phase noise of -120

dBc/Hz at offset of 1 kHz that is very close to our measured value from Fig. 17. We use 1 MHz for the slave laser linewidths, which is close to the measured linewidths of the DFB lasers used in the experiments. We assume the locking range is approximately 500 MHz and the detuning is 100 MHz. Fig. 29 shows that the phase noise at offsets close to carrier, such as 1 kHz or less, approximately follows the $20 \log(m)$ rule. For offsets further away from the carrier, such as 100 kHz or greater, the residual phase noise of the photonic synthesizer is the limiting factor.

We note that in practice, other broadband AM noise such as the noise of the RF amplifier following the photodetector may add additional noise. These results indicate that high-quality phase noise performance is achievable for the parameters appropriate to the devices used in the first concept demonstration of the Photonic Synthesizer. The analysis indicates that lower linewidth DFBs and wider mode spacing of the mode-locked laser, thus allowing for larger locking range, are both expected to improve the residual phase noise performance. Also, the use of a higher-quality RF reference oscillator will improve the absolute phase noise performance at low offset frequencies from the carrier.

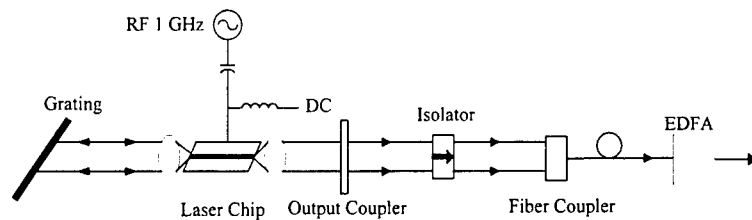


Figure 30: Schematic diagram of actively mode-locked external cavity semiconductor laser.

5 Experimental Results for Photonic Synthesizer Using Semiconductor Mode-Locked Laser

5.1 Construction of the semiconductor mode-locked laser

As we have discussed in the previous sections, the mode-locked laser is the heart of the Photonic Synthesizer. It is a critical component in the system and its performance directly influences the overall performance of the Photonic Synthesizer. Although developing a mode-locked laser suitable for the Photonic Synthesizer application was not the main goal of this project, the lack of a commercially-available mode-locked laser usable in the Photonic Synthesizer forced us to spend considerable time and effort to understand and optimize the mode-locked laser, and to engage in joint development with suppliers. In this section, we discuss the external-cavity semiconductor mode-locked laser used in the proof-of-concept Photonic Synthesizer experiments.

The semiconductor mode-locked laser has been the subject of extensive research for over a decade [38]-[44]. The motivation for research on semiconductor mode-locked lasers derives from the potential applications as a source of ultra short pulses for electro-optic sampling systems [45, 46], optical clock distribution [47, 48], and as a source for high speed data communication systems [49].

The external cavity mode-locked semiconductor used in this work was jointly developed with Sarnoff Research Center. Fig. 30 illustrates the configuration of the laser: it consists of a semiconductor laser amplifier, two collimating lenses, a grating reflector, an output coupler, an isolator, and a fiber-optic coupler.

The gain element is a multi-quantum well InGaAsP angled-stripe amplifier chip with anti-reflection coating (lower than 0.1% reflectivity) at both

facets. The chip is mounted p-side up on a copper stud cooled by a thermoelectric cooler (TEC) and controlled with a thermistor. Due to the angled-stripe design, the optical axis of the light is off-normal, at an angle of $\sim 21^\circ$, which reduces the tendency of the chip to lase off of its facets. The chip therefore acts as a superluminescent diode when forward biased, and the laser cavity is formed by the grating and output coupler, with longitudinal mode spacing determined by the cavity length.

The RF signal used to drive the mode-locked laser is a low phase noise source described previously. It is coupled to the chip through an RF bias tee and matching network. The chip was characterized using an RF network analyzer. It has a series resistance of around $2\ \Omega$ and a shunt capacitance of about 70 pF, resulting in very poor matching at 1 GHz. To improve the RF matching at 1 GHz, a microstrip matching circuit was fabricated from RT-Duroid and other RF components. The matching circuit enhances power transfer from the RF source to the chip in a narrow frequency range centered at 1 GHz. The microstrip circuit is mounted on a brass fixture that is clamped to the copper heat-sink stud of the gain chip.

The diffraction grating has 500 line/mm and reflectivity of 90%. It is mounted on a rotating stage, which allows adjustment of the wavelength reflected at its first order diffraction, which determines the center wavelength of the mode-locked laser. The tuning range exceeds 25 nm, limited by the laser amplifier chip gain bandwidth. Two lenses are used at either end of the chip to collimate the beam inside the cavity. The output mirror has reflectivity of around 20%, which was optimized to maximize the laser output power.

The external cavity length is approximately 15 cm, yielding a fundamental cavity spacing of 1 GHz. The length of the cavity is adjustable by a micrometer stage, to optimize alignment and to vary the detuning between the cavity and the 1 GHz RF source. To maintain the stability of the cavity modes, the optical components are mounted on an invar baseplate. Its resistance to thermal expansion provides stability of one part in 10^6 in the laboratory environment.

Outside the laser cavity, a free space optical isolator with 40 dB isolation is used to prevent any unwanted optical feedback to the laser. It was found that even a small amount of optical feedback can disturb the stable laser operation. The laser beam is then coupled to a polarization-maintaining fiber coupler with a GRIN lens with approximately 30% coupling efficiency.

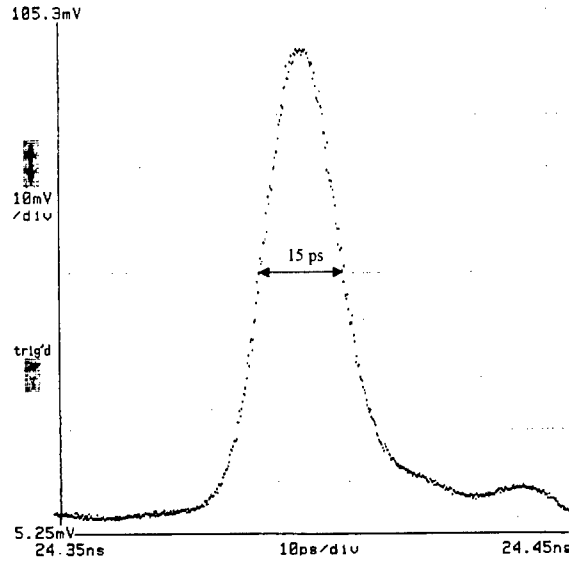


Figure 31: Pulse profile of the external cavity semiconductor mode-locked laser, showing the minimum pulse width is about 15 ps at zero detuning.

5.2 Performance of the semiconductor mode-locked laser

In this section, we report the performance of our semiconductor mode-locked laser, and discuss how to optimize the laser such that it yields the lowest phase noise.

First, the laser cavity is aligned for the maximum power output at a given current. The laser is biased just above threshold at 72 mA, which was found to yield the shortest pulse with lowest noise in the RF spectrum. The RF source delivers 25 dBm RF power to the input of the matching circuit to the laser. The average optical output power is 0.5 mW at these conditions. The optical power coupled to the fiber is only -8 dBm which is too low to perform many measurements, so an erbium-doped fiber amplifier (EDFA) is used to boost the power level to 14 dBm.

The output of the mode-locked laser is detected by a fast photo-detector with bandwidth of 45 GHz (New Focus model 1014). We use a Tektronix fast-sampling oscilloscope with sampling head bandwidth of 50 GHz to display the optical pulse. While observing this display, the laser cavity is tuned to achieve the minimum pulse width. We obtain the full width at half maximum (FWHM) of the optical pulse to be approximately 15 ps. Fig. 31

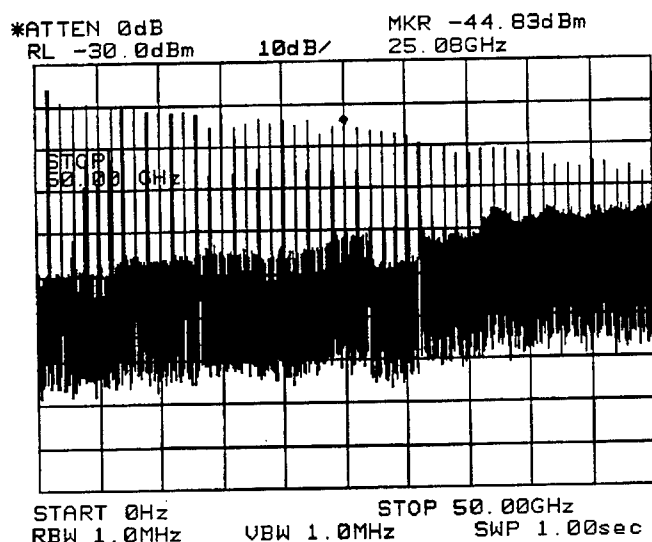


Figure 32: RF spectrum of the semiconductor mode-locked laser.

displays the pulse profile obtained on the oscilloscope. The minimum pulse width corresponds to the minimum detuning between the laser cavity mode spacing and the RF drive frequency.

The corresponding RF spectrum from direct detection of the laser pulse is shown in Fig. 32. The RF signal generated from the optical pulse of the mode-locked laser consists of a comb with 1 GHz spacing extending from 1 GHz fundamental frequency to 50 GHz and beyond. Due to the bandwidth of our photodetector and spectrum analyzer, we were not able to examine signals at frequencies higher than 50 GHz.

We can directly view the optical mode structure of the mode-locked laser using the Supercavity optical spectrum analyzer. Fig. 33 displays the profile of the mode structure. The profile is not a perfect Gaussian shape, but rather has amplitude modulation with a period of approximately 14 - 15 GHz; the reasons for such modulation are not fully understood and require further investigation, but it may be related to incomplete suppression of reflections in the laser cavity at the end-faces of the chip and lenses. The total number of modes is approximately 100 with mode spacing of 1 GHz.

We then measured the spectral bandwidth of the optical pulse using an HP70952B optical spectrum analyzer. The FWHM optical spectrum bandwidth is 0.23 nm. So the pulse width and frequency bandwidth product

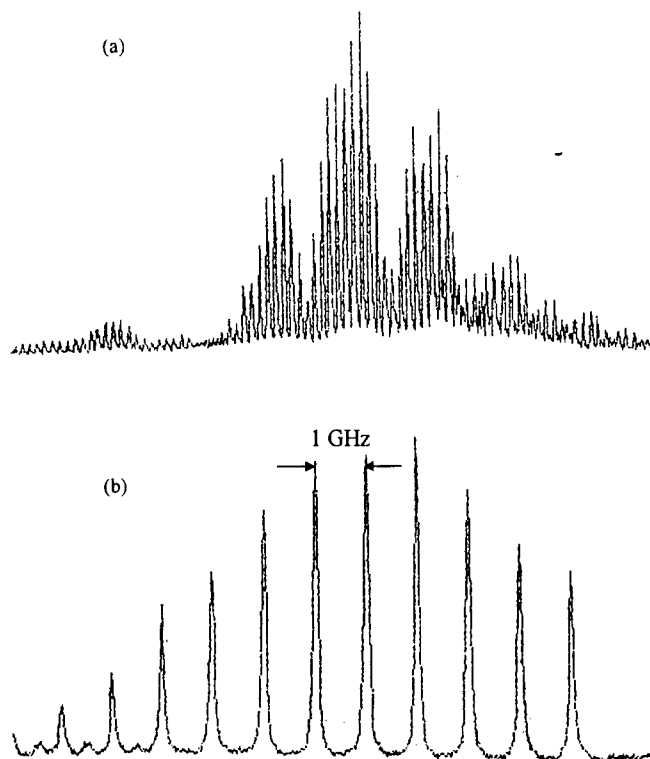


Figure 33: (a): mode structure of the semiconductor mode-locked laser viewed with a high-resolution Fabry-Perot optical spectrum analyzer; approximately 100 modes are visible with 1 GHz spacing. (b): a zoom view in which individual modes are resolved.

is 0.43, which is very close to the theoretical value of 0.441 for a Gaussian pulse profile, indicating that the mode-locked laser output pulse is very close to a Gaussian shape.

5.3 Phase noise and timing jitter of actively mode-locked laser

For many applications of mode-locked lasers, the timing jitter of the optical pulse must be minimized. For example, in electro-optic sampling, optical analog-to-digital conversion, and high speed digital transmission, the pulse-to-pulse timing jitter is critically important. Since the phase noise and timing jitter are closely related to each other, phase noise between 1 kHz to 100 kHz is usually important since the averaging times are typically in the range of milliseconds for most of measurements. For optical communication systems, the long term stability (> 1 second) of the optical pulse becomes important as well.

Due to the importance of the timing jitter, there are many theoretical [12, 13] [50]-[52] and experimental [11] [53]-[55] references on this topic. In the Photonic Synthesizer, because we use the mode-locked laser as a source to generate RF signals, the phase noise of the mode-locked laser directly translates to the phase noise of the resulting RF signal. Our goal is to minimize any phase noise degradation due to the mode-locked laser.

It was shown [12] that the resulting RF signal generated upon photodetection of the optical pulse output of the mode-locked laser may be written as

$$I(t) = \sum_{m=1}^N I_m \exp[-j\omega_R(mt + J_m(t))], \quad (68)$$

where I_m is the amplitude of the RF signal at frequency $m\omega_R$, where ω_R is the fundamental frequency of the mode-locked laser which is also the RF drive frequency, m is an integer, and $J_m(t)$ is a random variable representing the timing jitter. The relation between the timing jitter and the phase noise is

$$J_m(t) = \frac{m\delta\phi_R(t)}{\omega_R}, \quad (69)$$

where $\delta\phi_R(t)$ is a random variable representing the phase noise of the RF driving signal. Here, we assume that the mode-locked laser does not add

any phase noise to the signal above the RF drive signal phase noise. The timing jitter power spectral density of the m -th RF harmonic is then \sqrt

$$S_{J_m}(f) = \frac{m^2}{\omega_R^2} S_R(f), \quad (70)$$

where $S_R(f)$ is the phase noise power spectral density of the input RF drive signal. Eq.(70) implies that the RF phase noise at high harmonics is the multiplied phase noise of the fundamental RF drive signal. The rms pulse-to-pulse timing jitter is given by

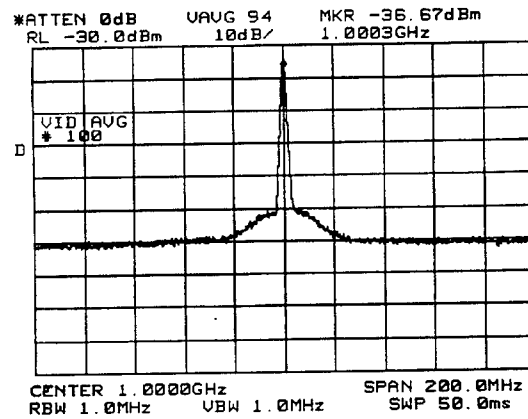
$$t_{rms} = \sqrt{\frac{2}{\omega_R^2} \int_{f_{min}}^{f_{max}} S_R(f) df}, \quad (71)$$

where the frequency integration limits of the phase noise depend on the measurement time scale.

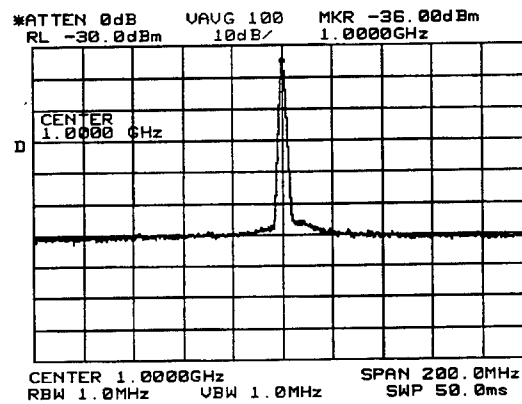
The timing jitter we discussed so far only considers the RF phase noise of the driving source. In addition, the mode-locked laser has spontaneous emission noise which will add to the overall phase noise. The added noise also strongly depends on the detuning between the laser cavity and the driving RF frequency, which we will discuss next. Technical noise sources such as DC bias-current fluctuations and vibrations of the optical mounts in the cavity may also result in timing fluctuations that exceed the value of the RF drive phase noise, but these may, in principle, be minimized with careful design.

In our investigations of the semiconductor external-cavity mode-locked laser, we observed that the minimum pulse width condition did not yield the lowest phase noise. The minimum pulse width of 15 ps occurs at zero detuning between the cavity frequency and the RF driving frequency. For positive detunings, the pulses become unstable and exhibit large timing jitter. Interestingly, when the detuning is slightly negative, about -2 MHz, we obtain the lowest phase noise, and the timing jitter is lowest. However, at -2 MHz detuning, the pulse is slightly broadened to about 22 ps. Further detuning the cavity to the negative side results in an even broader pulse with increasing phase noise, and the pulse eventually becomes asymmetrical with a slow trailing edge. For high enough negative detuning, the mode-locking is completely destroyed.

The RF spectrum of the mode-locked laser output at 1 GHz is shown in Fig. 34 for the cases of zero detuning and -2 MHz detuning. It is clear that the zero detuning case yields higher noise compared with the -2 MHz



(a)



(b)

Figure 34: Spectrum analyzer display of photodetected RF signal from mode-locked laser at 1 GHz. (a) the zero detuning case yields the shortest pulse width, but larger noise side bands compared with (b) the -2 MHz detuning case.

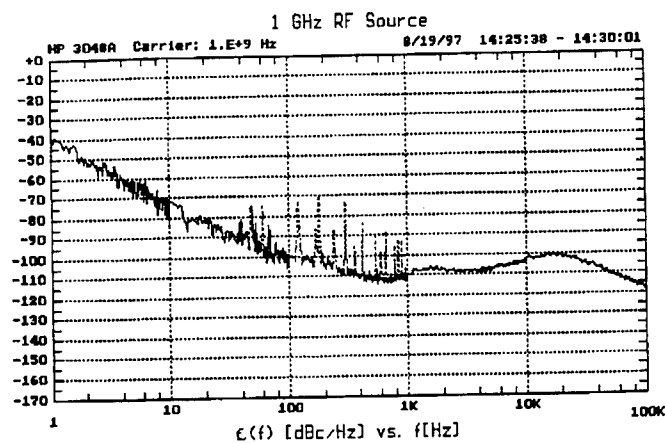
detuning case. Similar conclusions were reported in [44], in which numerical simulations based on a transmission-line laser model agreed well with observations of large cyclic instabilities in the pulse amplitude and timing when the detuning was in the positive range. Their experiments and numerical simulations were consistent with our observations.

An heuristic explanation of cyclic instabilities for the case of positive detuning can be given as follows: Because the RF drive frequency is larger than the cavity resonance frequency, the gain within the laser chip peaks before the return of the optical pulse from the external cavity. This means that the growth of a new pulse, preceding the returning pulse, is favored by the chip gain. The new pulse starts from spontaneous emission noise, and grows to dominance at the expense of the old pulse, because it receives more gain per round-trip. This process causes the apparent pulse position to jitter in time, leading to the observed large variations in the pulse shape and amplitude. These variations are manifested in the frequency domain as increased amplitude and phase noise sidebands.

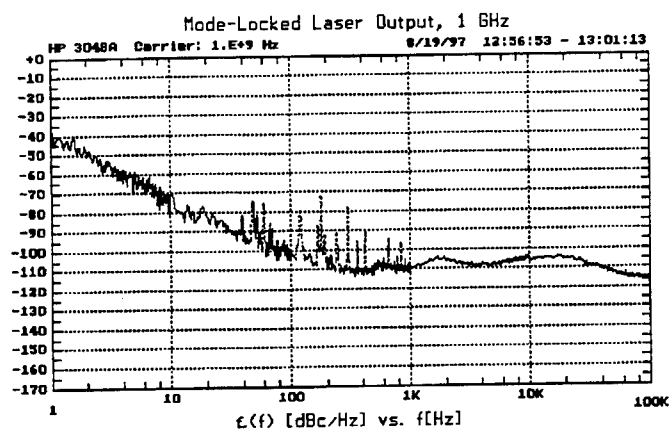
For slight negative detunings, the returning pulse reaches the chip just before the gain peaks. In this case, there is no growth of new pulses from noise. The returning pulse is regenerated through stimulated emission, so the overall pulse timing is firmly established by the driving RF source that modulates the chip gain. However, because the RF drive is off-frequency with the cavity resonance, fewer optical modes are phase-locked, resulting in increased pulsewidth. At zero detuning, the maximum number of modes are locked, yielding the shortest pulse width, but the uncertainty in the pulse timing is increased.

As we analyzed in a previous section, the linewidth of the injection-locked laser will be the same as the master laser linewidth. We use this fact to measure the linewidth of an individual mode of the mode-locked laser because it is difficult to filter out an individual mode using passive filters. To investigate this, we injection-locked a DFB laser to one mode of the mode-locked laser, and measured the linewidth of the locked CW DFB laser using a self-homodyne fiber delay-line setup. We obtained some interesting results: At zero detuning, we obtain the minimum pulse width, but the linewidth of the individual mode is approximately 3 MHz. At -2 MHz negative detuning, we obtain minimum phase noise in the RF spectrum, and the linewidth is reduced to only 0.5 MHz. We believe these results are the first direct observation of the linewidth of an individual mode in a mode-locked laser and its dependence on detuning. They may provide additional information for the further modeling of the mode-locked laser.

Phase noise measurements were performed with the laser adjusted for



(a)



(b)

Figure 35: (a) Phase noise of the 1 GHz RF drive source used in the mode-locked laser, (b) phase noise of the mode-locked laser output at 1 GHz, showing no measurable difference.

the lowest phase noise condition. Fig. 35 shows the phase noise of the mode-locked laser output at fundamental frequency 1 GHz, compared to the phase noise of the RF driving source. These phase noise measurements were taken using the HP 3048A phase noise test system. The phase noise of the mode-locked laser is virtually the same as the RF drive phase noise. This validated our previous assumptions in the mathematical treatment of the phase noise of the mode-locked laser.

Next, we performed a residual phase noise measurement for the mode-locked laser, illustrated in Fig. 36. In this measurement, the 1 GHz output signal from the mode-locked laser is mixed in phase quadrature (90 degree phase offset) with the RF drive signal in a phase detector. Since the RF driving source phase noise is common-mode on both phase detector ports, it is cancelled. The residual noise is then attributed to the mode-locked laser. The residual phase noise is due to fundamental laser spontaneous emission noise and other technical contributions such as cavity length fluctuation, DC bias source noise, etc. . The residual phase noise is relatively constant from frequency offsets of 10 Hz to 100 kHz. We believe that this is due to the laser spontaneous emission noise because this noise is broadband and its contribution in this frequency range is approximately constant. At frequencies close to the carrier from 10 Hz to 1 Hz, the residual phase noise is increasing. Given the relatively high sensitivity of the laser to alignment, this low frequency noise is likely due to laser cavity fluctuations influenced by the environment such as vibration, temperature changes, etc.

5.4 Photonic Synthesizer proof-of-concept demonstration using semiconductor mode-locked laser

To demonstrate the concept of the Photonic Synthesizer on the optical bench, we used the semiconductor mode-locked laser as the master laser to injection-lock two CW DFB lasers. Fig. 37 illustrates the experimental configuration. The output of the semiconductor laser was boosted to 14 dBm using an EDFA, then fed into the Photonic Synthesizer section. Instead of using circulators to direct the output of the CW DFB lasers, here we simply used two 10/90 fiber-optic couplers. Two mechanical optical attenuators were used to manually control the injection levels to the DFBs. The injection power levels were monitored using two 10% optical taps and optical power meters. The EDFA output was split into several paths for continuous monitoring of the mode-locked laser RF spectrum, optical spectrum, pulse profile, and mode structure during the experiment. Since the EDFA was constructed using non-polarization-maintaining fiber, the polarization

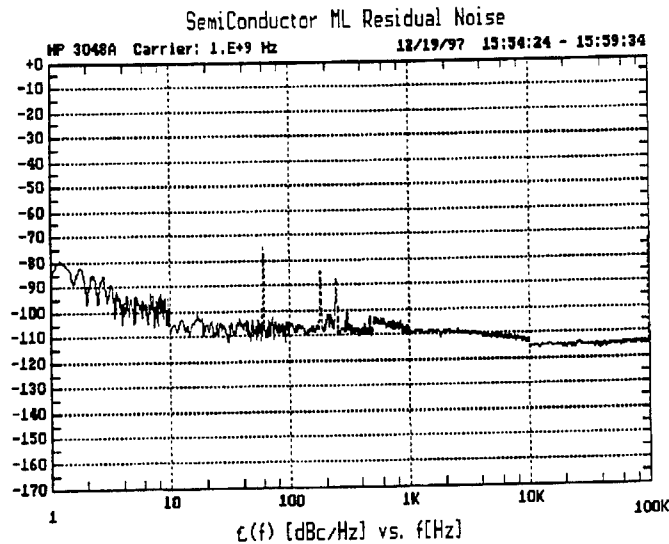


Figure 36: Residual phase noise of the semiconductor mode-locked laser at 1 GHz with RF driving source noise cancelled.

state of the EDFA output was undefined. Polarization-control paddles (not shown in the figure) were used to adjust the polarization input to the DFB lasers. The polarizing optical isolators insured that the light injected into the DFB lasers was linearly polarized.

The two DFB laser diodes were mounted on TO-5.6mm submounts attached to Peltier-cooler mounts. The DFBs were coupled into PM fibers using commercially available laser-to-fiber couplers with two lenses mounted on XYZ mechanical mounts with adjustable angle. The optical coupling efficiency achieved was approximately 50%. The mode-locked laser was injected into the two slave lasers through two 10/90 couplers. Three optical isolators minimized feedback from the slave lasers to the mode-locked laser. The main portions of the slave laser outputs were directed through another set of optical isolators before combining in a variable polarization-maintaining fiber coupler. These last two isolators minimized coupling of the DFB lasers to each other. The two optical paths were kept as equal as possible to minimize any phase noise-to-amplitude noise conversion due to path differences.

A high speed photodetector was used to detect the heterodyne output signal of the two slave lasers. A portion of the combined slave laser output was directed to a Supercavity optical spectrum analyzer to verify proper

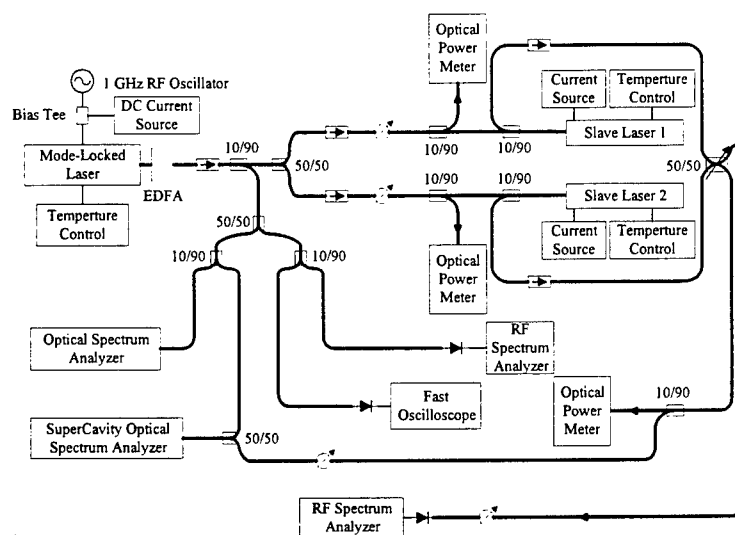


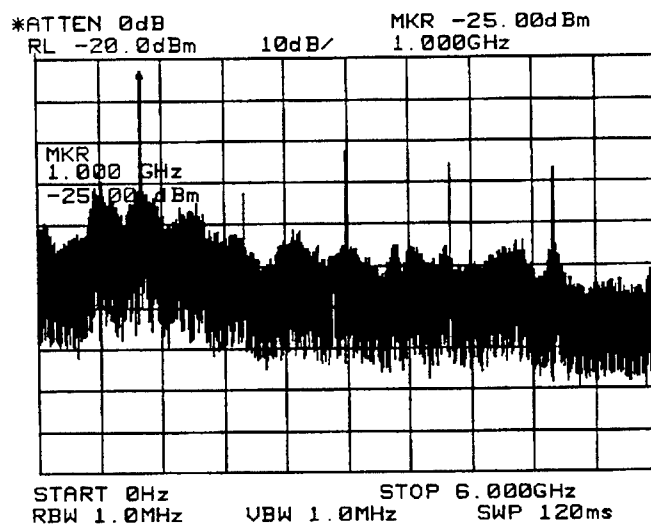
Figure 37: Block diagram of bench setup used for Photonic Synthesizer proof-of-concept demonstration using semiconductor external cavity mode-locked laser.

locking of the DFBs to the modes of the mode-locked laser. Two laser diode controllers were used to provide tuning of the DFB laser frequencies by changing the chip temperature and current. The laser frequency change with temperature was approximately 15 GHz/°C, and approximately 100 MHz/mA for current tuning.

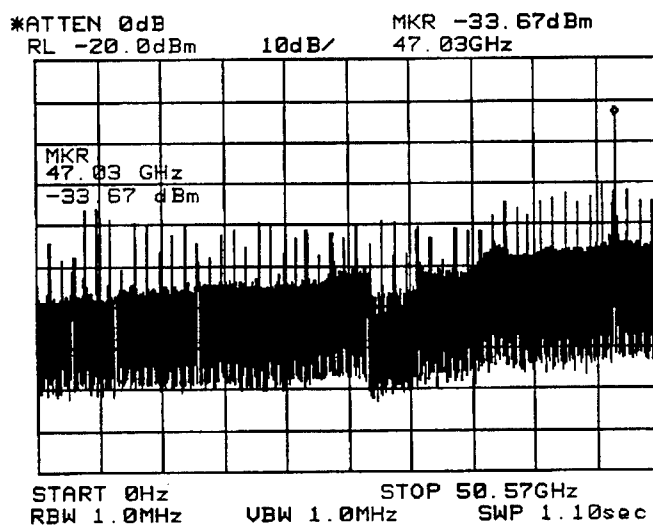
The two slave lasers were operated at approximately 100 mA. The synthesizer optical output power in the fiber was +10 dBm. The injected mode-locked laser average power was -13 dBm to -10 dBm. The peak power of the pulse was +4 dBm to +7 dBm. We estimate that the injected power of each individual mode was approximately -26 dBm, due to the power distribution across the optical comb. At these levels, the locking range was much less than the mode spacing of 1 GHz, and the slave lasers were therefore in the stable operating regime for injection-locking.

The heterodyne output signal could be tuned from 1 GHz to more than 50 GHz in steps of 1 GHz. Fig. 38 displays two examples of the Photonic Synthesizer detected heterodyne output signal at 1 GHz and at 47 GHz. Other modes of the mode-locked laser outside the injection-locking range introduced phase modulation to the injection-locked lasers, resulting in sidemodes that are about -15 dB or lower compared with the desired heterodyne signal. Fig. 39 shows a detailed view of these two signals to be pure, clean tones with low phase noise. The noise at high frequency increases as compared with low frequency signal as expected from the theoretical analysis.

Unfortunately, we were not able to keep the locking stable long enough to perform phase noise measurements using the HP3048A phase noise test system. The reason was due to the cavity length fluctuation of the mode-locked laser, which caused the optical comb to drift in the frequency domain. The slave lasers quickly lost lock in a matter of minutes as the drift was apparently greater than the locking range. To stabilize the mode-locked laser cavity further was beyond the scope of this research project. This points out that future research on the Photonic Synthesizer should include significant effort to develop stable, robust, and smaller mode-locked lasers.

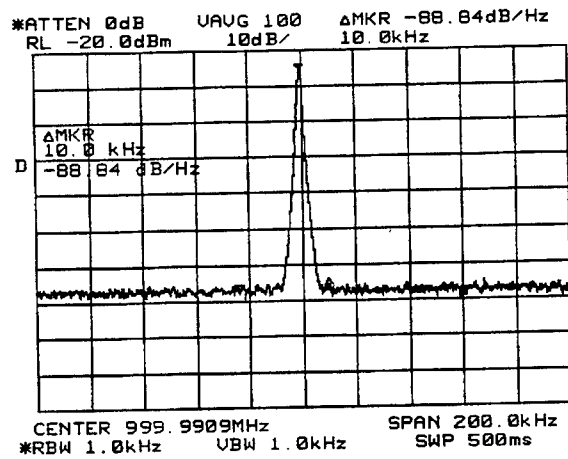


(a)

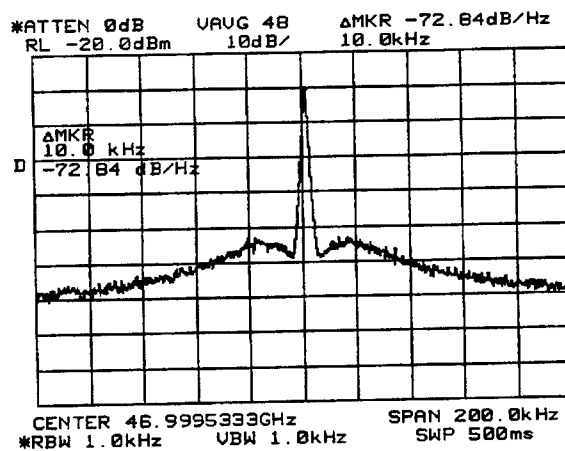


(b)

Figure 38: Signals generated from photonic synthesizer setup using the semiconductor mode-locked laser as master laser. (a) 1 GHz, (b) 47 GHz.



(a)



(b)

Figure 39: Zoom view of Fig. 38. (a) 1 GHz signal, (b) 47 GHz signal.

6 Photonic Synthesizer Experiments Using Fiber Mode-Locked Laser

While the semiconductor mode-locked laser enabled a proof-of-concept demonstration of the Photonic Synthesizer to be successfully conducted, it has several major drawbacks for this application. First, it was constructed using bulk free-space optical components and large mechanical mounts, so it was subject to sensitive alignment and required frequent adjustment to maintain optimum operation. Second, even when well-aligned, the cavity, mirrors, and gratings were very susceptible to mechanical vibrations and temperature fluctuations, which translated to added noise and frequency drift of the optical comb, making injection-locking possible for only a few minutes at a time. Third, due to these aspects, it would seem to be practically impossible to move the setup from an optical bench and package it into a standard rack unit and still maintain alignment during shipping and handling. In short, it was not a practical solution beyond the proof-of-principle demonstration. Since our further goal was to demonstrate that the Photonic Synthesizer could be used in practical situations, we turned our attention to an all-fiber approach employing an actively mode-locked erbium fiber ring laser. This laser has improved stability compared to the free-space semiconductor laser and afforded better experimental results. However, the fiber laser is still a sensitive instrument; true ruggedization of the Photonic Synthesizer will require further development effort directed toward the mode-locked laser.

6.1 Construction and performance of the fiber mode-locked laser

Fiber mode-locked lasers, both actively and passively locked, have attracted considerable interest recently [56]-[66]. One reason is that the fiber mode-locked laser, combined with intrinsic fiber nonlinearities such as self-phase-modulation, can yield very short pulses of sub-picosecond duration. Mode-locked erbium fiber lasers can produce transform-limited pulses at high repetition rates with wide tunability at commercially-interesting telecommunication wavelengths. They are also useful sources for high speed optical sampling and optical signal processing. Using harmonic mode-locking techniques, where the modulation frequency is an integral multiple of the fundamental laser cavity frequency, picosecond pulses with repetition rates greater than 20 GHz have been obtained. Fiber mode-locked lasers have found application in fiber soliton communication experiments, optical clock distribution, and all-optical switches.

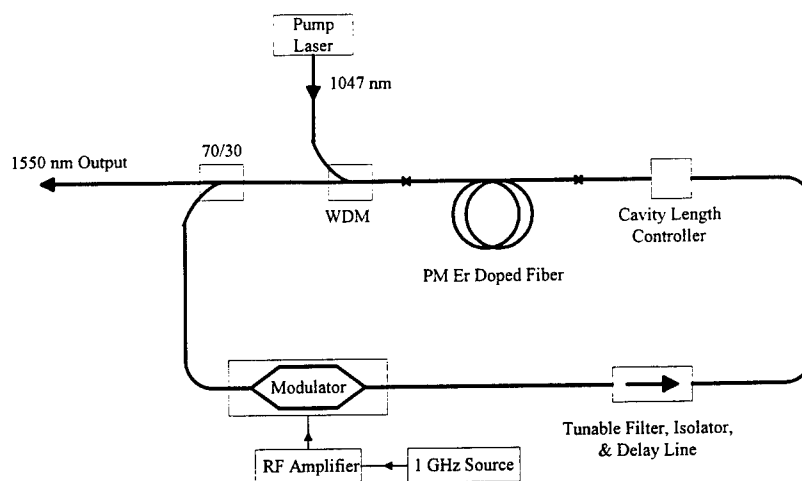


Figure 40: Schematic diagram of the fiber mode-locked laser used in the photonic synthesizer experiments.

The fiber mode-locked laser was supplied by Pritel, Inc. Fig. 40 shows the schematic diagram of the fiber mode-locked laser. It consists of a gain medium of Er-Yb co-doped polarization-maintaining fiber, a high power diode-pumped solid-state Nd:YLF pump laser, and a high speed MZ-modulator. The optical isolator is used to insure that the laser operates in one direction, a tunable filter is used to tune the laser center wavelength to the desired value within the erbium gain spectrum, a delay line is precisely cut to yield the multiple cavity frequency of 1 GHz, and a mechanical cavity length controller is used to manually adjust the cavity length for proper mode-locking. The fundamental cavity frequency of this laser is approximately 10 MHz. The optical filter has bandwidth of 0.8 nm. The laser cavity maintains single polarization through the use of polarization-maintaining components. An RF amplifier is used to amplify the drive signal to the MZ-modulator. The 1 GHz source is not included inside the laser package and must be provided by the user. In this case we used the 1 GHz source as described in Fig. 13.

The pump laser delivers approximately 700 mW at 1047 nm to the amplifier gain medium. The 1550 nm output is split to two ports. One port has polarization-maintaining fiber output with power level of 20 mW. This output is used in the Photonic Synthesizer to provide the injection-locking signal to the slave lasers. The other output is 40 mW and is used to monitor the performance of the mode-locked laser. The modulator bias and

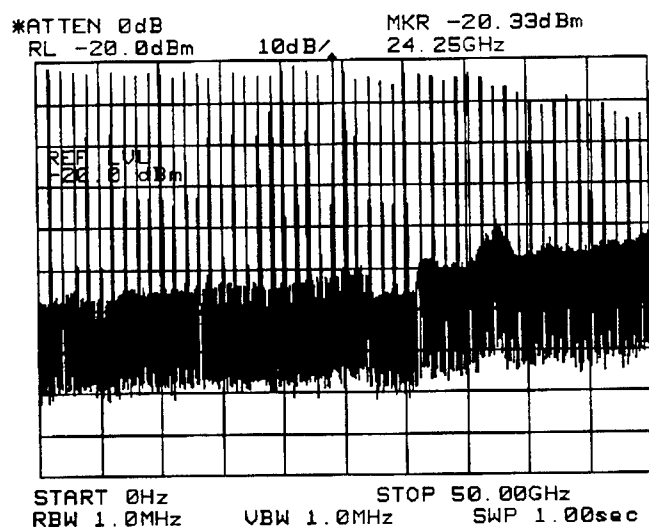
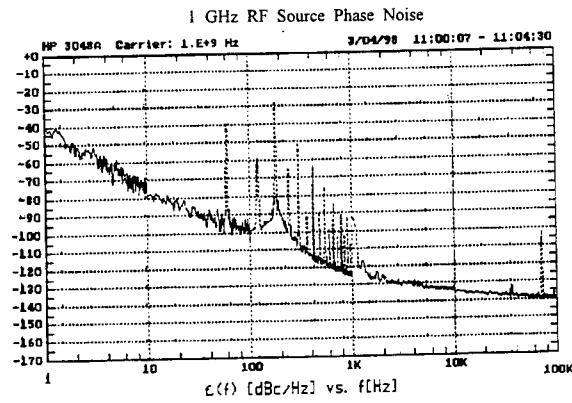


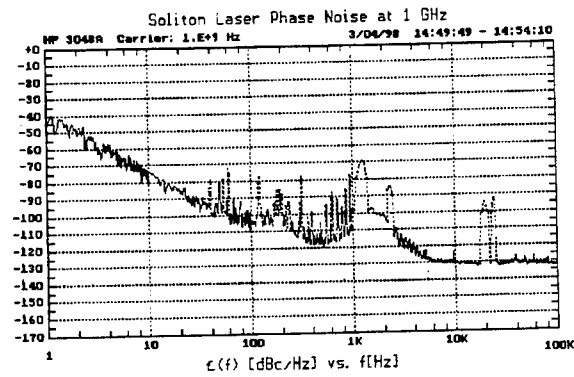
Figure 41: RF spectrum of fiber mode-locked laser. The harmonic amplitude roll-off at high frequencies is largely due to the photodetector frequency response roll-off.

cavity length require careful adjustment to yield optimum operation with minimum pulse width and phase noise. Optimization is achieved by monitoring the photodetected RF spectrum and adjusting the cavity length and modulator bias to maximize the sidemode suppression and minimize the RF noise sidebands. Autocorrelator measurements by the manufacturer obtain pulse widths smaller than 10 ps, which is beyond our photodetector -3dB bandwidth of 45 GHz. Fig. 41 displays the detected RF spectrum using our photodetector, showing RF tones from 1 GHz to 50 GHz in 1 GHz steps. The roll off at high frequencies is due to the frequency response of the photodetector. Compared with the same measurement of the semiconductor mode-locked laser in Fig. 32, the fiber mode-locked laser has much broader spectrum, indicating a shorter pulse width.

Fig. 42 shows the phase noise of the fiber mode-locked laser at 1 GHz, compared with the phase noise of the driving RF source at 1 GHz (same as displayed in Fig. 17). The phase noise of the fiber mode-locked laser and its driving RF source are the same for frequencies below 10 kHz. At offset frequencies of 10 kHz and higher, there is excess broadband amplitude noise contribution from the mode-locked laser and RF drive and post-detection amplifiers. There is also an unidentified noise contribution from 1 kHz to



(a)



(b)

Figure 42: (a) Phase noise of the 1 GHz RF source, (b) phase noise of the fiber mode-locked laser at 1 GHz.

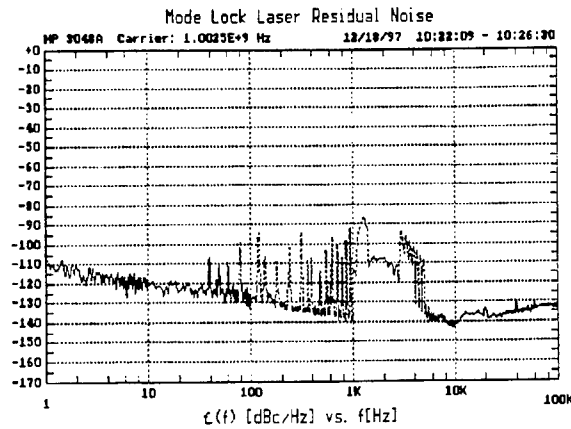


Figure 43: Residual phase noise of the fiber mode-locked laser at 1 GHz with RF driving source noise cancelled.

3 kHz range from the mode-locked laser. The source of this noise may be the internal DC supplies for the RF amplifier or optical modulator, but could not be conclusively identified due to limited access to the internal construction of the mode-locked laser. In Fig. 43, we plot the residual phase noise of the fiber mode-locked laser in which the 1 GHz driving source phase noise has been cancelled as discussed previously. The technical noise in the range of 1 kHz to 3 kHz is clearly visible, but the remaining noise floor is as much as 30 dB lower than the semiconductor mode-locked laser residual noise previously plotted in Fig. 36. This is the basis of the improved phase noise performance of the Photonic Synthesizer using the fiber vs. the semiconductor mode-locked laser. However, this does not imply that a semiconductor mode-locked laser has intrinsically poorer performance than a fiber laser; it was simply beyond the scope of this research program to develop an improved semiconductor mode-locked laser.

6.2 Performance of the Photonic Synthesizer using fiber mode-locked laser

In this section we present the experimental results of the Photonic Synthesizer with the fiber mode-locked laser as the source. The test setup was displayed in Fig. 18 and discussed previously. The setup block diagram is repeated again in Fig. 44. The experimental setup is similar to that used with the semiconductor mode-locked laser, described in Section 71. How-

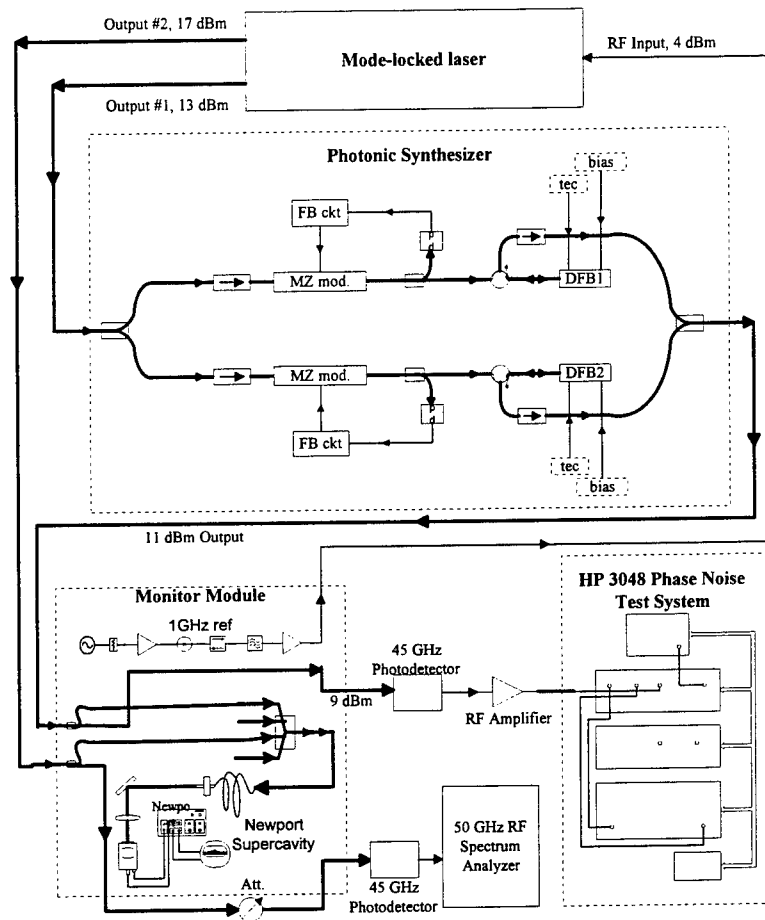


Figure 44: Experimental setup of the photonic synthesizer using the fiber mode-locked laser.

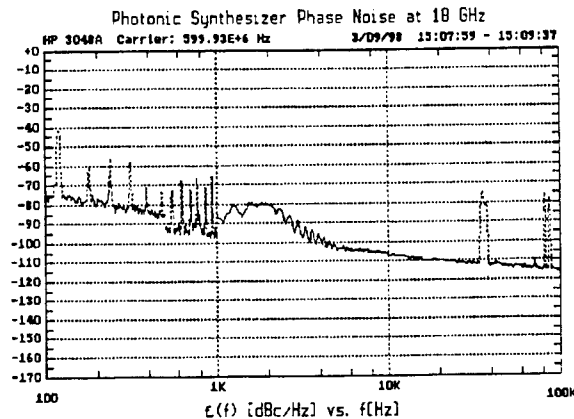
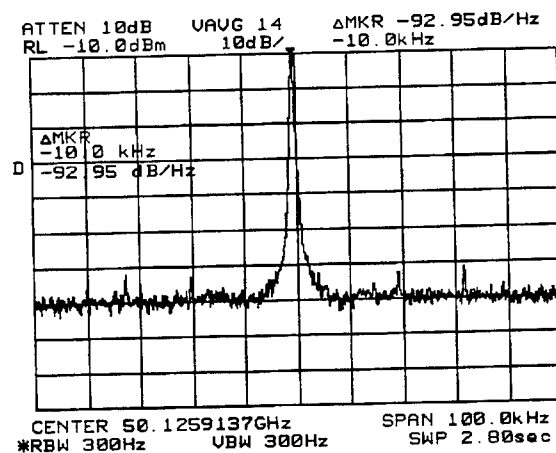


Figure 45: Phase noise of the photonic synthesizer at 18 GHz using the fiber mode-locked laser. The signal is down-converted to 600 MHz and measured using the HP3048A phase noise test system.

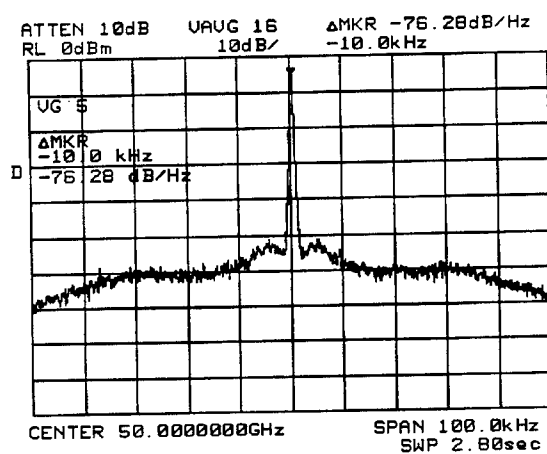
ever, in this case, optical circulators were used to couple power into and out of the slave lasers instead of the 10% couplers. This improved the optical output power and the optical isolation of the slave lasers.

The tuning strategy was described previously in Section 71. We were able to tune the Photonic Synthesizer from 1 GHz to approximately 100 GHz in 1 GHz steps. However, due to the bandwidth limitation of our photodetector to approximately 50 GHz, we are not able to directly detect signal higher than 50 GHz.

The Photonic Synthesizer phase noise was directly measured at frequencies from 1 GHz to 50 GHz, which was the upper frequency limitation of the measurement system. Fig. 45 shows an example of Photonic Synthesizer phase noise at 18 GHz measured using the HP3048 phase noise test setup. At 10 kHz offset, the phase noise is -108 dBc/Hz, which is approximately 10 dB higher than the theoretical prediction of Eq. 66 displayed in Fig. 28 for the case of 500 MHz locking bandwidth. It could be the case that the locking bandwidth was actually less in this measurement, resulting in a higher value of residual phase noise that would explain the discrepancy. Regardless, these measurements demonstrate that the Photonic Synthesizer is capable of generating ultra-wide bandwidth signals from 1 GHz to 50 GHz and beyond, with phase noise performance in reasonable agreement with the theoretical model. This validates the use of the theoretical model we have



(a)



(b)

Figure 46: Millimeter wave signal at 50 GHz, (a) signal generated from photonic synthesizer, (b) signal obtained from HP 83650L synthesizer.

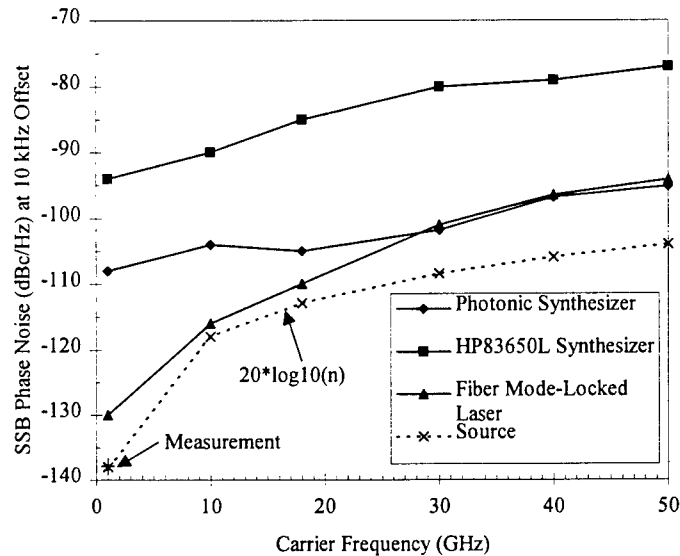


Figure 47: Comparison of RF phase noise at 10 kHz offset from carrier at different frequencies for: photonic synthesizer, HP 83650L commercial synthesizer, fiber mode-locked laser, and RF driving source. The RF source phase noise plot at frequencies > 1 GHz was calculated from the 1 GHz data according to the theoretical multiplication formula $20 \log(n)$.

developed as a design aid to predict and optimize the Photonic Synthesizer performance.

For the purposes of comparison, we also performed phase noise measurements on a Hewlett-Packard HP83650L synthesizer which is tunable from 10 MHz to 50 GHz, and represents the commercial state-of-the-art for wideband signal synthesizers. Fig. 46 shows the 50 GHz output from the Photonic Synthesizer compared to the HP 83650L synthesizer, showing that the Photonic Synthesizer yields lower noise. In this case, the noise at 10 kHz offset from the carrier is -93 dBc/Hz for the Photonic Synthesizer, and -76 dBc/Hz for the HP83650L synthesizer, or about 17 dB higher.

The phase noise was measured for the fiber mode-locked laser, Photonic Synthesizer, and HP 83650L synthesizer at frequencies of 1 GHz, 10 GHz, 20 GHz, 30 GHz, 40 GHz, and 50 GHz. Fig. 47 summarizes the phase noise results for these sources at 10 kHz offset from the carrier. The results

indicate that the Photonic Synthesizer has at least 15 dB lower phase noise compared with HP 83650L over the range of 1 GHz to 50 GHz. The Photonic Synthesizer follows the phase noise of the fiber mode-locked laser at frequencies of 30 GHz and higher, as expected. The Photonic Synthesizer exhibited excess phase noise at lower frequencies relative to the fiber mode-locked laser. For frequencies less than 20 GHz, the measured phase noise of the Photonic Synthesizer was approximately constant in the range of -105 to -108 dBc/Hz. A constant residual phase noise floor versus carrier frequency is predicted by the theory in Eq. 66, and plotted in Fig. 29. We also plot the ideal multiplied phase noise from the RF driving source at 1 GHz according to the formula $20 \log_{10} n$, where n is the multiplication factor, which represents the lower limit to phase noise performance. The measured Photonic Synthesizer performance was approximately 10 dB worse than predicted by Eq. 66 and plotted in Fig. 29. This discrepancy may be due to incorrect assumptions made in the theoretical analysis, due to the difficulty of quantifying exactly parameters such as the detuning and locking range of the lasers, etc. Resolution of this discrepancy was beyond the scope of this research program, and would be a logical topic to address in future research. However, given the complexity of the system and the multiple possibilities for extraneous noise sources to degrade the performance, the agreement between theory and experiment was quite reasonable and serves to validate the Photonic Synthesizer concept as a means of producing widely tunable, low phase noise signals.

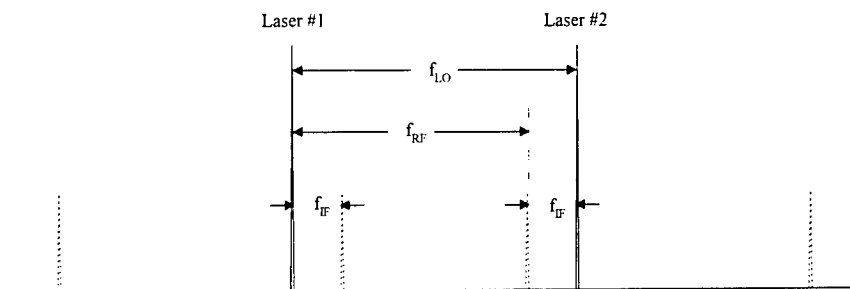


Figure 48: Block diagram of photonic down-converter experiment using photonic synthesizer. The injection-locked slave lasers with frequency separation f_{LO} are modulated using a high-speed MZ-modulator by input signal frequency f_{RF} ; the photodetected output is the down-converted input signal at intermediate frequency $f_{IF} = f_{LO} - f_{RF}$.

7 Millimeter-wave Photonic Frequency Conversion Using Photonic Synthesizer

In this Section, we demonstrate an application of the Photonic Synthesizer as the optical local oscillator in a millimeter-wave photonic down-converter.

Photonic down-conversion eliminates the electronic mixer to convert millimeter-wave signals directly to lower frequency RF signals in one step. This has potential applications in antenna applications and high frequency analog transmission [4]-[8]. Photonic downconversion can also be realized by using cascaded optical modulators [6],[7]. In the cascaded modulator scheme, a high frequency mm-wave signal is needed to provide the local oscillator (LO) signal in order to downconvert the input (RF) signal to the desired intermediate frequency (IF) signal. By using the Photonic Synthesizer as the optical LO source, the need for the high frequency mm-wave signal and second optical modulator to generate the LO is eliminated, so only one high-frequency modulator is required. The Photonic Synthesizer provides an ideal source for the optical LO signal that is phase-coherent with a low-frequency reference oscillator.

Fig. 48 illustrates the principle of photonic downconversion using the Photonic Synthesizer in the optical frequency domain. The two heterodyned lasers (laser #1 and laser #2) from the Photonic Synthesizer with frequency separation of f_{LO} form the optical LO signal, which is passed through a high speed MZ-modulator. The optical LO signal is then modulated by

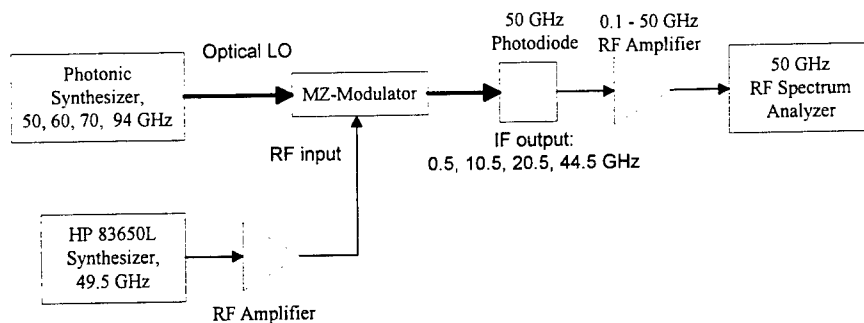


Figure 49: Block diagram of photonic down-converter experiment using photonic synthesizer as the optical local oscillator, and a wideband 50 GHz optical modulator as the photonic mixer. The input signal is generated by the HP83650L synthesizer.

the RF input signal at frequency f_{RF} . The modulation process produces two optical sidebands on each of the DFB laser frequencies at $\pm f_{RF}$. Upon photodetection, the upper modulation sideband of laser #1 beats with the carrier of laser #2 to generate the downconverted signal at frequency $f_{IF} = f_{LO} - f_{RF}$; the same is true for the lower modulation sideband of laser #2 beating with the carrier of laser #1. By low-pass filtering the photodetector output, the higher frequency products at f_{LO} , f_{RF} , $f_{LO} + f_{RF}$, etc. are filtered out. Note that the photodiode need only respond to frequencies up to f_{IF} , which may be at baseband, although the input signal is a millimeter-wave frequency.

Fig. 49 illustrates the experimental setup used to demonstrate mm-wave photonic downconversion. The output of the Photonic Synthesizer is launched into a high speed MZ-modulator [67] that had -3 dB bandwidth of approximately 45 GHz. The HP83650L synthesizer was used as the RF source; its output was amplified to provide enough modulation index for the MZ-modulator. The output frequency of the HP synthesizer was maintained at 49.5 GHz. The optical output of the modulator was detected using a high speed photodiode, followed by a broadband RF amplifier, then displayed on a 10 MHz to 50 GHz RF spectrum analyzer. The RF output at 49.5 GHz from the photodiode was -33 dBm after the amplifier.

With the Photonic Synthesizer tuned to 50 GHz, a 0.5 GHz IF signal is generated with output power of -36.3 dBm, which is only 3.3 dB less than the detected RF signal at 49.5 GHz. The phase noise of the IF signal at 0.5 GHz

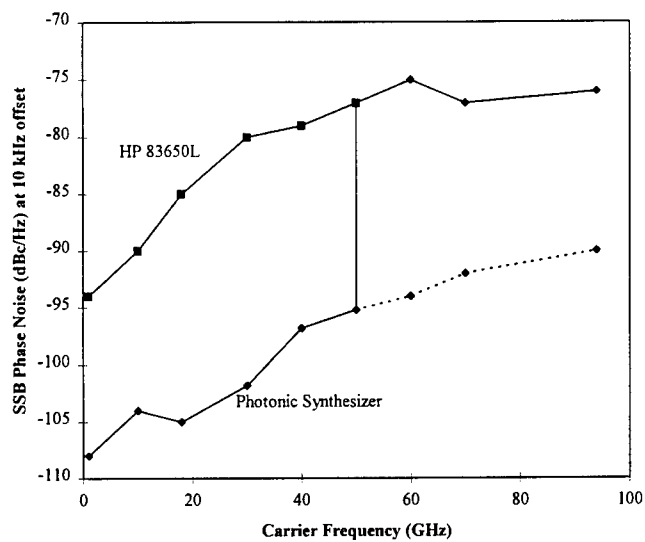


Figure 50: Photonic synthesizer phase noise including the phase noise measurements at high frequencies of 60 GHz, 70 GHz, and 94 GHz. The phase noise is dominated by the HP 83650L synthesizer which is used as the input signal source for the downconverter experiments. The dashed line is the predicted phase noise of the photonic synthesizer based on the phase noise at 50 GHz and extended using the ideal $20 \log(n)$ formula.

was -77 dBc/Hz at 10 kHz offset. This phase noise was equal to the phase noise of the HP83650L synthesizer phase noise for 49.5 GHz carrier. From previous experiments, we know that the Photonic Synthesizer phase noise is -95 dBc/Hz at 50 GHz, therefore, the IF signal phase noise is dominated by the HP83650L synthesizer. To demonstrate wideband optical frequency conversion, the Photonic Synthesizer was then tuned to frequencies of 60 GHz, 70 GHz, and 94 GHz, resulting in IF signals at 10.5 GHz, 20.5 GHz, and 43.5 GHz, respectively. The phase noise measurements at these frequencies are about the same, around -76 dBc/Hz, again confirming our expectation that the IF phase noise is dominated by the HP synthesizer rather than by the Photonic Synthesizer. Fig. 50 displays the phase noise measurements for the Photonic Synthesizer from 1 GHz to 94 GHz. The dashed line after 50 GHz indicates the likely phase noise of the Photonic Synthesizer based on a $20 \log_{10} n$ extrapolation of the phase noise measurement at 50 GHz. This indicates that the high phase noise above 50 GHz measured using the downconverter method was limited by HP83650L synthesizer.

These experiments demonstrate the capability of photonic downconversion as an extremely wideband signal processing technique, and the usefulness of the Photonic Synthesizer as an enabling technology to realize ultra-wideband signal generation, distribution, and processing in optical fiber systems.

8 Summary and Conclusions

A Photonic Synthesizer based on the heterodyne combination of two DFB lasers injection-locked to an actively mode-locked laser was studied theoretically and experimentally. Low phase noise RF, microwave, and millimeter-wave signals were generated using the Photonic Synthesizer from 1 GHz to 94 GHz in 1 GHz steps. The phase noise of the synthesizer at 50 GHz was less than -95 dBc/Hz at 10 kHz offset from the carrier, which is more than 17 dB lower than the phase noise of state-of-the art commercial frequency synthesizers at this frequency.

We performed a detailed theoretical analysis of injection-locking of semiconductor DFB lasers. The injection-locking range and stability analysis were reviewed, and our experiments agreed well with the theoretical results. The phase noise of the injection-locking was also studied in detail, and its relation to injection-locking range, detuning, and laser linewidth were analyzed. We derived the residual phase noise of the Photonic Synthesizer which predicts the fundamental limitation of the phase noise for this system.

We constructed an optical bench system using a combination of free-space optics and optical fiber-coupled components, and used it to demonstrate the proof-of-concept of the Photonic Synthesizer. The results obtained with the optical bench system were used to aid the design and construction of the final deliverable Photonic Synthesizer, which was realized using all fiber-coupled components.

The final deliverable Photonic Synthesizer was packaged in a 19" rack with temperature stabilization for the critical optical components. Control software to tune the synthesizer was written using LabView running on a laptop PC that is an integral part of the synthesizer system. We performed experiments using the Photonic Synthesizer and obtained high quality tunable RF signals from 1 GHz to 94 GHz.

A diagnostic system was also constructed using a Newport Supercavity optical spectrum analyzer to monitor the mode-locked laser and Photonic Synthesizer performance, and as a tool to aid in the tuning of the Photonic Synthesizer. A low phase noise 1 GHz RF source was constructed and used as the reference signal for the actively mode-locked laser.

We spent considerable effort to build a semiconductor mode-locked laser in cooperation with Sarnoff Research Center. In designing the setup of this laser, we studied the characteristics of semiconductor mode-locked laser, the locking range, pulse profile, and phase noise. We were able to measure the linewidth of individual modes of the optical comb of a mode-locked laser, for the first time to our knowledge, using the injection-locking tech-

nique. The results provide some interesting insight regarding semiconductor mode-locked laser behavior. Improved performance was obtained using an Er:Yb fiber mode-locked laser (Pritel, Inc.) that had lower phase noise and higher output power. Finally, we demonstrated an application of the Photonic Synthesizer as the optical local oscillator in a millimeter-wave photonic frequency-converting link for RF signals over the frequency range from 1 GHz to 94 GHz.

The results of this research project validate experimentally and theoretically the Photonic Synthesizer concept. The mode-locked laser proves to be the most important subsystem in the Photonic Synthesizer. In order to build a robust, small, and less-expensive Photonic Synthesizer, a small, reliable, and robust mode-locked laser is needed. Future research should be directed to designing and constructing such a laser, and to miniaturizing the Photonic Synthesizer optical circuitry. The Photonic Synthesizer may find many potential applications in antenna systems, RF signal distribution, and RF analog signal processing.

References

- [1] R.T.Logan Jr., "Photonic Radio-Frequency Synthesizer," Photonics and Radio Frequency, Brian M. Hendrickson, Editor, Proc. SPIE 2844, pp.312-317, 1996.
- [2] U.Gliese, T.N.Nielsen, M.Bruun, E.Lintz Christensen, K.E.Stubkjær, S.Lindgren, and B.Broberg, "A wideband heterodyne optical phase-locked loop for generation of 3-18 GHz microwave carriers", *IEEE Photon. Technol. Lett.*, vol.4, pp.936-938 (1992).
- [3] R.T.Logan, X.S.Yao, G.F.Lutes, "Photonic signal processing and transmission", *NASA/Jet Propulsion Laboratory New Technology Report*, NPO-19437, 11, April 1994.
- [4] R.T. Logan Jr. and E. Gertel, "Millimeter-wave photonic downconvertors: theory and demonstrations", Proc. SPIE Conf. on Optical Technology for Microwave Applications VII, Vol. 2560, San Diego CA, July 9-14, 1995, pp. 58-69.
- [5] J. O'Reilly and P. Lane, "Remote delivery of video services using mm-waves and optics", *J. Lightwave Technol.*, vol. 12, pp. 369-375 (1994).
- [6] C.K. Sun, R.J. Orazi, S.A. Pappert, and W. K. Burns, "A photonic-link millimeter-wave mixer using cascaded optical modulators and harmonic carrier generation", *IEEE Photon. Technol. Lett.*, vol.8, pp. 1166-1168 (1996).
- [7] G. K. Gopalakrishnan, W. K. Burns and C. H. Bulmer, "Microwave-optical mixing in LiNbO₃ modulators", *IEEE Trans. Microwave Theory Tech.*, vol. 41, p. 2383-2391, 1993.
- [8] K.P. Ho, S.K. Liaw, and C. Lin, "Efficient photonic mixer with frequency doubling", *IEEE Photon. Technol. Lett.*, vol. 9, pp. 511-513 (1997).
- [9] M.Kasevich and S.Chu, *Phys.Rev.Lett.* vol. 69, 1741 (1992).
- [10] P. Bouyer, T.L. Gustavson, K.G. Haritos, and M.A. Kasevich, "Microwave signal generation with optical injection locking", *Opt.Lett.* vol. 21, 1502 (1996).

- [11] J.E. Bowers, P.A. Morton, A. Mar, and S.W. Corzine, "Actively mode-locked semiconductor lasers", *IEEE J. Quantum Electron.*, vol. QE-25, 1426 (1989).
- [12] D.R. Hjelme and A.R. Mickelson, "Theory of timing jitter in actively mode-locked lasers", *IEEE J. Quantum Electron.*, vol. QE-28, 1594 (1992).
- [13] P.T. Ho, "Phase and amplitude fluctuations in a mode-locked laser", *IEEE J. Quantum Electron.*, vol. QE-21, 1806-1813 (1985).
- [14] K. Kikuchi, C.-E. Zah, and T.-P. Lee, "Amplitude-modulation side-band injection locking characteristics of semiconductor lasers and their application", *J. Lightwave Technol.*, vol. 6, 1821-1930 (1988).
- [15] M. Chamberland, M. Têtu, and P. Tremblay, "Spectral characterization of microwave signals generated by the heterodyne of injection-locked semiconductor lasers", in "Optoelectronic Signal Processing for Phased Array Antennas IV, Proc. 2155", B.M. Hendrickson. ed., SPIE, Bellingham (1994).
- [16] P. Gallion, H. Nakajima, G. Debarge, and C. Chabran, "Contribution of spontaneous emission to the linewidth of an injection-locked semiconductor laser", *Electron. Lett.*, vol. 21, 626 (1985).
- [17] B. van der Pol, "Forced oscillations in a circuit with non-linear resistance," *Philosophical Mag.*, vol. iii, 65-80 (1927).
- [18] R. Adler, "A study of locking phenomena in oscillators," *Proc. IRE*, vol. 34, 351-357 (1946).
- [19] K. Kurokawa, "Injection locking of microwave solid-state oscillators," *Proc. IEEE*, vol. 61, 1386-1410 (1973).
- [20] G. Lidoyne, P. Gallion, C. Chabran, and G. Debarge, "Locking range, phase noise and power spectrum of an injection-locked semiconductor laser", *IEE Proceedings*, Vol.137, 147 (1990).
- [21] K. Otsuka and S. Tarucha, "Theoretical studies on injection locking and injection-induced modulation of laser diodes", *IEEE J. Quantum Electron.*, vol. QE-17, 1515-1521 (1981).
- [22] K. Kobayashi, H. Nishimoto, and R. Lang, "Experimental observation of asymmetric detuning characteristics in semiconductor laser injection locking," *Electron. Lett.*, vol. 18, 54-56 (1982).

- [23] C. L. Tang and H. Statz, "Phase-locking of laser oscillators by injected signal," *J. Appl. Phys.*, vol. 38, 323-324 (1967).
- [24] R. H. Pantell, "The laser oscillator with an external signal," *Proc. IEEE*, vol. 53, 474-477 (1965).
- [25] R. Lang, "Injection locking properties of a semiconductor laser," *IEEE J. Quantum Electron.*, vol. QE-18, 976-983 (1982).
- [26] F. Mogensen, H. Olesen, and G. Jacobsen, "Locking conditions and stability properties for a semiconductor laser with external light injection," *IEEE J. Quantum Electron.*, vol. QE-21, 1515-1521 (1985).
- [27] I. Petitbon, P. Gallion, G. Debarge, and C. Chabran, "Locking bandwidth and relaxation oscillations of an injection-locked semiconductor laser," *IEEE J. Quantum Electron.*, vol. QE-24, 148-154 (1988).
- [28] R. Hui, "Optical PSK modulation using injection-locked DFB semiconductor lasers," *IEEE Photon. Technol. Lett.*, vol. 2, pp. 743-746 (1990).
- [29] R. Hui, A. D'Ottavi, A. Mecozzi, and P. Spano, "Injection locking in distributed feedback semiconductor lasers," *IEEE J. Quantum Electron.*, vol. QE-27, 1688-1695 (1991).
- [30] A. Umbach, G. Unterborsch, R. P. Braun, and G. Großkopf, "Stable optical source and high-speed photodetector used for remote fiber-optic 64-GHz mm wave generation," in *Optical Fiber Communication Conference*, vol. 2, 1998 OSA Technical Digest Series (Optical Society of America, Washington, D.C., 1998), pp. 260-261.
- [31] T. B. Simpson, J. M. Liu, and A. Gavrielides, "Bandwidth enhancement and broadband noise reduction in injection-locked semiconductor lasers," *IEEE Photon. Technol. Lett.*, vol. 7, pp. 709-711 (1995).
- [32] S. Mohrdiek, H. Burkhard, and H. Walter, "Chirp reduction of directly modulated semiconductor lasers at 10 Gb/s by strong CW light injection," *J. Lightwave Technol.*, vol. 12, pp. 418-424 (1994).
- [33] G. Yabre, "Effect of relatively strong light injection on the chirp-to-power ratio and the 3 dB bandwidth of directly modulated semiconductor lasers," *J. Lightwave Technol.*, vol. 14, pp. 2367-2373 (1996).
- [34] J. M. Liu, H. F. Chen, X. J. Meng, and T. B. Simpson, "Modulation bandwidth, noise, and stability of a semiconductor laser subject

- to strong injection locking," *IEEE Photon. Technol. Lett.*, vol. 10, pp. 1325-1327 (1997).
- [35] T. B. Simpson and J. M. Liu, "Enhanced modulation bandwidth in injection-locked semiconductor lasers," *IEEE Photon. Technol. Lett.*, vol. 9, pp. 1322-1324 (1997).
 - [36] J. Sacher, D. Baums, P. Panknin, W. Elsässer, and E. O. Göbel, "Intensity instabilities of semiconductor lasers under current modulation, external light injection, and delayed feedback", *Phys. Rev. A*, vol. 45, 1893-1905 (1992).
 - [37] V. Annovazzi-Lodi, S. Donati, and M. Manna, "Chaos and locking in a semiconductor laser due to external injection", *IEEE J. Quantum Electron.*, vol. QE-30, 1537-1541 (1994).
 - [38] P. T. Ho, "Coherent pulse generation with GaAlAs laser by active mode locking", *Electron. Lett.*, vol. 5, 526 (1979).
 - [39] A. Olsson and C. L. Tang, "Active mode locking of linear and ring external-cavity semiconductor lasers", *IEEE J. Quantum Electron.*, vol. QE-17, 1977-1978 (1981).
 - [40] K. Y. Lau and A. Yariv, "Direct modulation and active mode locking of ultrahigh speed GaAlAs lasers at frequencies up to 18 GHz," *Appl. Phys. Lett.*, vol. 46, 326 (1985).
 - [41] R. S. Tucker, S. K. Korotky, G. Eisenstein, U. Koren, L. W. Stulz, and J. J. Veselka, "20 GHz active mode-locking of a 1.55 μm InGaAsP laser," *Electron. Lett.*, vol. 21, 239 (1985).
 - [42] R. S. Tucker, U. Koren, G. Raybon, B. I. Miller, T. L. Koch, and G. Eisenstein, "40 GHz active mode-locking in a 1.5 μm monolithic extended cavity laser," *Electron. Lett.*, vol. 25, 621 (1989).
 - [43] P. J. Delfyett, C. -H. Lee, G. A. Alphonse, and J. C. Connolly, "High peak power picosecond pulse generation from AlGaAs external cavity mode-locked semiconductor laser and traveling-wave amplifier," *Appl. Phys. Lett.*, vol. 57, 971 (1990).
 - [44] A. J. Lowery, N. Onodera, and R. S. Tucker, "Stability and spectral behavior of grating-controlled actively mode-locked lasers," *IEEE J. Quantum Electron.*, vol. QE-27, 2422-2430 (1991).

- [45] J. A. Valdmanis, G. A. Mourou, and C. W. Gabel, "Picosecond electro-optic sampling system," *Appl. Phys. Lett.*, vol. 41, 211 (1982).
- [46] K. J. Weingarten, M. J. W. Rodwell, and D. M. Bloom, "Picosecond optical sampling of GaAs integrated circuits," *IEEE J. Quantum Electron.*, vol. QE-22, 79-93 (1986).
- [47] P. J. Delfyett, D. H. Hartman, and S. Z. Ahmad, "Optical clock distribution using a mode-locked semiconductor laser diode system," *J. Lightwave Technol.*, vol. 9, pp. 1646-1694 (1991).
- [48] T. Ono, T. Shimizu, Y. Yano, and H. Yokoyama, "Optical clock extraction from 10 Gbit/s data pulses by using monolithic mode-locked laser diodes," in *OFC Tech. Dig.*, San Diego, CA, 1995, paper ThL4.
- [49] H. Shi, P. J. Delfyett, G. A. Alphonse, and J. C. Connolly, "20×5 Gbit/s optical WDM-TDM transmitter using a single-stripe multiwavelength mode-locked semiconductor laser," in *Optical Fiber Communication Conference*, vol. 2, 1998 OSA Technical Digest Series (Optical Society of America, Washington, D.C., 1998), pp. 311.
- [50] H. A. Haus and A. Mecozzi, "Noise of mode-locked laser," *IEEE J. Quantum Electron.*, vol. QE-29, 983-996 (1993).
- [51] I. G. Fuss, "An interpretation of the spectral measurement of optical pulse train noise," *IEEE J. Quantum Electron.*, vol. QE-30, 2707-2710 (1994).
- [52] L. -P. Chen, Y. Wang, J. -M. Liu, "Spectral measurement of the noise in continuous-wave mode-locked laser pulses," *IEEE J. Quantum Electron.*, vol. QE-32, 1817-1825 (1996).
- [53] M. J. W. Rodwell, D. M. Bloom, and K. J. Weingarten, "Subpicosecond laser timing stabilization," *IEEE J. Quantum Electron.*, vol. QE-25, 817-827 (1989).
- [54] K. A. Williams, I. H. White, D. Burns, and W. Sibbett, "Jitter reduction through feedback for picosecond pulsed InGaAsP lasers," *IEEE J. Quantum Electron.*, vol. QE-32, 1988-1994 (1996).
- [55] P. Langlois, D. Gay, N. McCarthy, and M. Piché, "Noise reduction in a mode-locked semiconductor laser by coherent photon seeding," *Opt. Lett.* vol. 23, 114 (1998).

- [56] J. D. Kafka, T. Baer, and D. W. Hall, "Mode-locked erbium-doped fiber laser with soliton pulse shaping," *Opt.Lett.* vol. 14, 1269-1271 (1989).
- [57] H. Takara, S. Kawanishi, M. Saruwatari, and K. Noguchi, "Generation of highly stable 20 GHz transform-limited optical pulses from actively mode-locked Er-doped fiber lasers with an all-polarization maintaining ring cavity," *Electron. Lett.*, vol. 28, 2095-2096 (1992).
- [58] D. Burns and W. Sibbett, "Controlled amplifier modelocked Er fiber ring laser," *Electron. Lett.*, vol. 26, 505-506 (1990).
- [59] H. Takara, S. Kawanishi, and M. Saruwatari, "20 GHz transform-limited optical pulse generation and bit-error-free operation using a tunable actively modelocked Er-doped fiber ring laser," *Electron. Lett.*, vol. 29, 1149-1150 (1993).
- [60] X. Shan and D. M. Spirit, "Novel method to suppress noise in harmonically modelocked erbium fiber lasers," *Electron. Lett.*, vol. 29, 979-981 (1993).
- [61] G. T. Harvey and L. F. Mollenauer, "Harmonically mode-locked fiber ring laser with an internal Fabry-Perot stabilizer for soliton transmission," *Opt.Lett.* vol. 18, 107-109 (1993).
- [62] J. S. Wey, J. Goldhar, D. W. Rush, M. W. Chbat, G. M. Carter, and G. L. Burdge, "Performance characterization of a harmonically mode-locked erbium fiber ring laser," *IEEE Photon. Technol. Lett.*, vol. 7, pp. 152-154 (1995).
- [63] J. S. Wey, J. Goldhar, and G. L. Burdge, "Active harmonic modelocking of an erbium fiber laser with intracavity Fabry-Perot filters," *J. Lightwave Technol.*, vol. 15, pp. 1171-1180 (1997).
- [64] I. N. Duling, III, "Subpicosecond all-fiber erbium laser," *Electron. Lett.*, vol. 27, 544-545 (1991).
- [65] D. J. Richardson, R. I. Laming, D. N. Payne, M. W. Phillips, and V. J. Matsas, "320 fs soliton generation with passively mode-locked erbium fiber laser," *Electron. Lett.*, vol. 27, 730 (1991).
- [66] K. Tamura, L. E. Nelson, H. A. Haus, and E. P. Ippen, "Soliton versus nonsoliton operation of fiber ring lasers," *Appl. Phys. Lett.*, vol. 64, 149-151 (1994).

- [67] Two integrated-optical modulators were tried with similar results: one device was a commercially-available device available from Sumitomo Cement Corporation (Japan) graciously loaned to us by Dr. Ed Ackerman of MIT Lincoln Laboratory, while the other was a device fabricated by Dr. W. Burns of Naval Research Laboratory.

Acronyms

ALC	automatic level control
AM	amplitude modulation
Att	attenuator
CW	continuous-wave
DARPA	Defense Advanced Research Projects Agency
dB	decibel, unit expressing the ratio between two amounts, for power $dB=10 \log_{10}(P_1/P_2)$
dBc	dB unit of relative power with the carrier power as the reference level
dBm	a measure of power defined as $dBm= 10 \log_{10} \frac{\text{power (milliwatts)}}{1 \text{ milliwatt}}$
DC	direct current
DFB	distributed-feedback
DUT	device under test
EDFA	erbium-doped fiber amplifier
Er:Yb	Erbium:Ytterbium
FB	feed back
FDM	frequency-division-multiplex
FWHM	full width at half maximum
GaAlAs	Gallium Aluminum Arsenic
Gb/s	Gigabytes (1×10^9 bytes) per second
GHz	Gigahertz (1×10^9 hertz)
GRIN	Gradient Index (lens)
HP	Hewlett-Packard
Hz	hertz (1 cycle, unit of frequency)
IEEE	Institute of Electrical and Electronics Engineers
IF	intermediate frequency
IRE	Institute of Radio Engineers
kHz	Kilohertz (1×10^3 hertz)
km	Kilometer (1×10^3 Meters)
LNA	low noise amplifier
LFP	low pas filter
LO	local oscillator
MIT	Massachusetts Institute of Technology
MHz	Megahertz (1×10^6 hertz)
mA	milliamphere (1×10^{-3} Ampere)
mW	milliwatt (1×10^{-3} Watts)
MZ	Mach Zehnder
Nd:YLF	actually (ND:LiYF ₄) Neodymium: Lithium Yttrium Fluoride
Nd:YAG	Neodymium: Yttrium Aluminum Garnet
nm	nanometer (1×10^{-9} Meter)
OIC	optical integrated circuit
PLL	phase-locked loop
PM	polarization-maintaining
ps	picoseconds (1×10^{-12} Seconds)
PSD	Power Spectral Density
PSK	phase shift keying
RIN	relative intensity noise
RF	radio frequency
SPAWAR	Space and Navel Warfare Systems Command
SPIE	Society of Photo-Optical Instrumentation Engineers
SSB	single sideband
TEC	thermoelectric cooler
XYZ	three orthogonal directions (in – out, left – right, up –down)
°C	degrees Celsius
Ω	ohm, unit of electric resistance

DISTRIBUTION LIST

addresses	number of copies
AIR FORCE RESEARCH LABORATORY/SNDR JAMES NICTER 25 ELECTRONIC PKY ROME NY 13441-4515	6
UNITED TELECOMMUNICATIONS PRODUCTS TRANSMISSION SYSTEM DIVISION 500 HORIZON DR STE 502 CHALFONT PA 18914	5
AFRL/IFOIL TECHNICAL LIBRARY 26 ELECTRONIC PKY ROME NY 13441-4514	1
ATTENTION: DTIC-OCC DEFENSE TECHNICAL INFO CENTER 8725 JOHN J. KINGMAN ROAD, STE 0944 FT. BELVOIR, VA 22060-6218	1
DEFENSE ADVANCED RESEARCH PROJECTS AGENCY 3701 NORTH FAIRFAX DRIVE ARLINGTON VA 22203-1714	1
ATTN: NAN PFRIMMER IIT RESEARCH INSTITUTE 201 MILL ST. ROME, NY 13440	1
AFIT ACADEMIC LIBRARY AFIT/LDR, 2950 P. STREET AREA B, BLDG 642 WRIGHT-PATTERSON AFB OH 45433-7765	1
AFRL/MLME 2977 P STREET, STE 6 WRIGHT-PATTERSON AFB OH 45433-7739	1

AFRL/HESC-TDC 1
2698 G STREET, BLDG 190
WRIGHT-PATTERSON AFB OH 45433-7604

ATTN: SMDC IM PL 1
US ARMY SPACE & MISSILE DEF CMD
P.O. BOX 1500
HUNTSVILLE AL 35807-3801

TECHNICAL LIBRARY D0274(PL-TS) 1
SPAWARSSYSCEN
53560 HULL ST.
SAN DIEGO CA 92152-5001

COMMANDER, CODE 4TL000D 1
TECHNICAL LIBRARY, NAWC-WD
1 ADMINISTRATION CIRCLE
CHINA LAKE CA 93555-6100

CDR, US ARMY AVIATION & MISSILE CMD 2
REDSTONE SCIENTIFIC INFORMATION CTR
ATTN: AMSAM-PD-OB-R, (DOCUMENTS)
REDSTONE ARSENAL AL 35898-5000

REPORT LIBRARY 1
MS P364
LOS ALAMOS NATIONAL LABORATORY
LOS ALAMOS NM 87545

ATTN: D'BORAH HART 1
AVIATION BRANCH SVC 122-10
FOB10A, RM 931
800 INDEPENDENCE AVE, SW
WASHINGTON DC 20591

AFIWC/MSY 1
102 HALL BLVD, STE 315
SAN ANTONIO TX 78243-7016

ATTN: KAROLA M. YOURISON 1
SOFTWARE ENGINEERING INSTITUTE
4500 FIFTH AVENUE
PITTSBURGH PA 15213

USAF/AIR FORCE RESEARCH LABORATORY
AFRL/VSOSA(LIBRARY-BLDG 1103)
5 WRIGHT DRIVE
HANSCOM AFB MA 01731-3004

1

ATTN: EILEEN LADUKE/D460
MITRE CORPORATION
202 BURLINGTON RD
BEDFORD MA 01730

1

OUSD(P)/DTSA/DUTD
ATTN: PATRICK G. SULLIVAN, JR.
400 ARMY NAVY DRIVE
SUITE 300
ARLINGTON VA 22202

1

AIR FORCE RESEARCH LAB/SND
25 ELECTRONIC PKY
ROME NY 13441-4515

1

JOANNE L. ROSSI
AIR FORCE RESEARCH LAB/SNW
25 ELECTRONIC PKY
ROME NY 13441-4515

1

ROBERT T. KEMERLEY
AIR FORCE RESEARCH LABORATORY/SND
2241 AVIONICS CIRCLE, RM C2G69
WRIGHT-PATTERSON AFB OH 45433-7322

1